Fork Reversal Safeguards Epigenetic Inheritance during DNA Replication Under Stress

Qiong Wu[1,3], Caixian Zhou[1,3], Yue Dou[2], Nadia I. Martin[2], Maria Gwit[2], Roséa Chen[1], Ke Zhu[1], Tianpeng Zhang[1], Shangming Tang[2], Tian Zhang[2], Tyler Weaver[2], Wenpeng Liu[1,2,4]*

[1]Department of Radiation Oncology, School of Medicine, University of Virginia, Charlottesville, VA 22908, USA.

[2]Department of Biochemistry and Molecular Genetics, School of Medicine, University of Virginia, Charlottesville, VA 22908, USA.

[3]These authors contributed equally

[4]Lead Contact

*Correspondence: W. L. xbg5zt@virginia.edu

Abstract

During DNA replication, epigenetic information carried by histone modifications is faithfully propagated and re-established on sister chromatids, ensuring cell identity. DNA replication is tightly coupled to chromatin reassembly, therefore perturbations to DNA replication compromise epigenetic inheritance fidelity; however, the underlying mechanisms remain poorly understood. In this study, we reveal a critical role for replication fork reversal in maintaining the transmission of epigenetic information under replication stress. We show that cells defective in fork reversal exhibit reduced nucleosome density at replication forks, accompanied by the loss of parental histones during their transfer onto nascent DNA. Mechanistically, we showed that PrimPol activation leads to single-stranded DNA gaps in fork reversal deficient cells; PARylation and DNA–protein crosslinking on single-stranded DNA subsequently evicts nucleosomes. Our

findings demonstrate that replication fork reversal, a widespread physiological process, is essential not only for preserving genome integrity but also for safeguarding epigenome stability.

Introduction

In eukaryotic cells, DNA replication is not merely the duplication of genetic material; it is also a critical process for the faithful transmission of epigenetic information[1]. During each S phase of the cell cycle, DNA must be precisely duplicated, and chromatin structure must be accurately reassembled to ensure cell identity, gene expression programs, and overall genome stability[2,3]. This chromatin-based inheritance, referred to as epigenetic information, encompasses histone modifications, DNA methylation, and the regulation by non-coding RNAs[4]. Programmed regulation of epigenetic states is essential for cell differentiation and organismal development[5], whereas aberrant epigenetic changes can drive diseases and tumorigenesis[6-9]. In cancer therapy, instability of the epigenetic landscape exacerbates tumor cell heterogeneity and promotes drug resistance[10]. Therefore, elucidating the mechanisms that safeguard epigenetic stability during DNA replication is of fundamental importance.

During DNA replication, nucleosomes ahead of the fork are disassembled by the FACT (FAcilitates Chromatin Transcription) complex into one H3–H4 tetramer and two H2A–H2B dimers, which are subsequently recycled to their original positions on sister chromatids by multiple histone chaperones after DNA replication[1,11-19]. With the assistance of histone chaperones, like ASF1 and CAF1, recycled parental histones are incorporated together with newly synthesized histones to assemble nucleosomes on nascent DNA[1,20-31]. Post-translational modifications (PTMs) on parental histones serve as templates that are copied onto adjacent new histones through a “read–write” mechanism, thereby completing the replication of epigenetic

information[1,32-36]. Replication-associated factors such as MCM2, PCNA, DNA polymerases ε/α, and fork protection proteins including Tof1, Mrc1, Csm3, and Ctf4 contribute to parental histone transfer[24-26,34,37-47]. As a result, DNA replication exerts profound influence on epigenetic stability. For example, deletion of Pol E3/E4, subunits of leading-strand polymerase ε, causes enrichment of parental histones (i.e. H3K9me3) on the lagging strand, thereby activating expression of the normally repressed LINE-1 (Long Interspersed Element-1) retrotransposon[48]. Conversely, mutations in lagging-strand histone chaperones, such as MCM2-2A, lead to parental histone accumulation on the leading strand[37,38]. Simultaneous disruption of both leading- and lagging-strand histone chaperones results in the loss of parental histones and their modifications, impairing stem cell differentiation[49].

DNA replication frequently encounters obstacles such as complex structured DNA, transcription–replication conflicts, repetitive sequences, and common fragile sites (CFSs)[3,50]. Replication stress induces multiple response pathways, including fork uncoupling, ATR activation, and replication fork reversal[3,50]. Among these, the generation of single-stranded DNA (ssDNA) and fork reversal are the two most common structural intermediates, occurring in diverse cell types in response to various forms of replication stress[51]. Our previous work and those of others have shown that ssDNA can be processed by RAD51-mediated strand invasion together with multiple fork remodelers, including SMARCAL1, ZRANB3, and HLTF, to form reversed forks[51-62]. This process stabilizes replication intermediates and prevents excessive ssDNA accumulation and subsequently fulfills the proper DNA replication. When fork reversal is impaired, cells activate PrimPol to reinitiate DNA synthesis downstream of the leading strand—a process known as repriming[63,64]. Although replication can resume, this generates

abundant ssDNA gaps on nascent DNA, posing a threat to chromatin structure and genome stability[65-67].

While the roles of ssDNA and fork reversal in genome stability have been well studied, their impact on epigenetic stability during replication remains blank. Most existing studies on DNA replication and epigenetics focus on unperturbed conditions[30,31,34,37-39,41,42,47-49,68], while rarely about stressed condition [1]. It is unclear whether and how, under replication stress, fork reversal or ssDNA gaps influence parental histone recycling and nucleosome assembly. This question is particularly relevant in the context of "difficult-to-replicate" genomic regions—such as repetitive sequence regions—which account for over half of the genome and are prone to persistent replication stress, where fork reversal should occurs frequently[69]. In this case, the replication fork is in a dynamic of stalled, repair and restart. Although slow, the fork still moving forward. The epigenetic features of these regions must be faithfully inherited during replication to modulate transcription; however, how replication stress responses—particularly fork reversal—affect the epigenetic inheritance in these regions is not yet clear.

In this study, we demonstrate that replication fork reversal promotes parental histone recycling and nucleosome assembly on sister chromatids by suppressing ssDNA formation, thereby preserving epigenetic stability. In cells lacking fork reversal, activation of the PrimPol primase leads to repriming, generating ssDNA gaps that result in the loss of parental histones and their modifications. Mechanistically, ssDNA triggers PARP1-mediated PARylation and HMCES-dependent DNA–protein crosslink formation, both of which inhibit nucleosome assembly. Our findings reveal a critical role for replication fork reversal in safeguarding epigenetic stability under replication stress.

Results

Replication fork reversal deficiency reduces nucleosome density on nascent DNA under replication stress

To investigate the impact of replication fork reversal on nucleosome assembly at replication forks, we performed SILAC-iPOND-MS (Stable Isotope Labeling by Amino acids in Cell Culture - Isolation of Proteins on Nascent DNA - Mass Spectrometry) analysis in wild type (WT) U2OS cells and fork reversal enzymes, including SMARCAL1, HLTF, ZRANB3, knockout cells (termed as FRKO) to examine protein composition on nascent DNA, upon hydroxyurea (HU)-induced replication stress (Figure 1A). Compared with wild-type cells, fork reversal–deficient cells exhibited decreased abundance of nearly all histones on nascent DNA. In contrast, the levels of the MCM2–7 helicase complex remained unchanged, indicating that histone reduction was not due to a decrease in replication fork number (Figure 1A), nor reduced replication progression, as measured by EdU (5-Ethynyl-2'-deoxyuridine) incorporation (Figure S1A). Immunofluorescence analysis of total chromatin-bound histone H3 showed no difference between fork reversal–deficient and wild-type cells (Figure S1B–E), suggesting that histone loss was restricted to nascent DNA.

To validate the mass spectrometry results, we pulse labeled nascent DNA with EdU, induced replication stress with HU, and quantified histone H3 on nascent DNA using a proximity ligation assay (PLA). Since fork reversal–deficient cells incorporate EdU more rapidly than wild-type cells (Figure S1A), direct comparison of PLA signals would not accurately reflect histone abundance (Figure 1B, 1C). Therefore, we normalized PLA signals to EdU intensity, yielding a value representing histone abundance per unit length of replicated DNA (Figure 1D). Using this

approach, we observed reduced H3 levels on nascent DNA in fork reversal–deficient cells, consistent with the proteomics results (Figure 1A). This reduction was observed across different HU concentrations (Figure S1F). The PLA analyses of H2A, H2B, and H4 were consistent with those for H3 (Figure 1B-D, Figure S1A), indicating reduced nucleosome density on nascent DNA rather than loss of individual histone types (Figure S1G–I).

We further validated these results using ChOR (Chromatin Occupancy after Replication)-seq, a high-throughput sequencing technique that profiles the occupancy of histone (modifications) and chromatin-associated proteins on newly replicated DNA[70], which confirmed a significant reduction in histone H3 abundance on nascent DNA in fork reversal–deficient cells (Figure 1E–G, Figure S1J), consistent with the proteomic and PLA results.

These experiments were performed in U2OS cells with triple knockout of SMARCAL1, ZRANB3, and HLTF. Since each fork reversal enzyme has unique functions independent of fork reversal, we tested whether the low nucleosome density phenotype was due to the fork reversal mechanism itself or to specific functions of individual enzymes. PLA analysis of single-knockout U2OS cells for each enzyme, including FBH1 knockout, revealed decreased histone abundance at replication forks in all cases (Figure S2A–B). Consistent with observations in FRKO cells, knockdown of RAD51, also an essential factor for fork reversal, led to reduced histone abundance at replication forks (Figure 1H and Figure S2C). In the absence of HU treatment, PLA and ChOR-seq showed no reduction in H3 levels in fork-reversal–deficient cells (Figure S2D-F), supporting that histone loss arises specifically under replication stress.

Altogether, the data indicate that fork reversal machinery maintains nucleosome density during replication under persistent stressed condition (Figure S2G).

Replication fork reversal deficiency leads to parental histone loss and chromatin decompaction

During DNA replication, parental histones positioned ahead of the fork are disassembled and subsequently recycled onto daughter DNA through highly coordinated mechanisms, where they combine with newly synthesized histones to form nucleosomes. Under conditions of persistent replication stress, the reduced nucleosome density observed on nascent DNA in fork reversal–deficient cells may arise from either impaired parental histone recycling or defective incorporation of new histones, both of which threaten faithful epigenetic inheritance. Importantly, the deposition of certain histone variants, such as CENP-A, macroH2A, and H3.3, occurs independently of DNA replication [71-73]. Thus, detection of these variants on nascent DNA reflects inheritance of parental histones, and their loss can be attributed to defective parental histone recycling (Figure 1A).

Previous studies have shown that certain histone modifications, such as di- and trimethylation of H3K9, H3K27, H3K79, and H4K20, are established on new histones many hours post-replication or even during the subsequent cell cycle, making them markers of parental histones during replication[30,38,48,49,68,74,75]. To assess whether parental histone recycling was impaired, we combined iPOND-MS with propionylation treatment to examine histone modifications at replication forks (Figure 2A). Upon HU-induced replication stress, parental histone–specific marks such as H4K20me2, H3K79me2, H3K27me3, and H3K9me3 were markedly reduced on nascent DNA in fork reversal–deficient cells (Figure 2B, Figure S3A-D). Consistent with this, marks characteristic of newly synthesized histone modifications—such as H4K5ac, H3K56ac, H4K12ac, H3K9ac, and H3K9me1[48,68]—were increased or unchanged (Figure 2B, Figure S3E-I). PLA assays corroborated the mass spectrometry findings (Figure 2C, Figure S3L). These

results suggest loss of parental histones during transmission, with a modest increase in new histone incorporation that only partially compensates for the loss, leading to an overall reduction in nucleosome density on nascent DNA.

To distinguish whether the reduction of H3K9me3 arises from replication stress or from preexisting global changes, we performed immunofluorescence analysis. A slight decrease in global H3K9me3 was observed only in 3KO cells following HU treatment (Figure 2D–E; Figure S3M–N), indicating that the loss of this repressive mark in fork reversal–deficient cells is specifically attributable to replication stress.

H3K9me3 and H3K27me3 are parental histone–specific marks that also indicate compact chromatin. We also detected a decrease in the abundance of another compaction marker, H3K9me2 on nascent DNA in fork reversal–deficient cells (Figure 2B, 2F), while global cellular H3K9me2 levels remained unchanged after HU treatment (Figure S3O-R). These findings are consistent with our model in which nucleosome density is reduced.

Proteomics data showed loss of H3K9me3, macroH2A.1, macroH2A.2 and reduced CENP-A (Figure 1A, Figure 2B). CENP-A marks alpha-satellite DNA at centromeres, macroH2A.1, macroH2A.2 are deposited in broad chromatin, with a strong bias toward facultative heterochromatin; H3K9me3 is a major component of constitutive heterochromatin and is typically enriched at repetitive genomic elements to suppress their transcription. Our findings indicate that heterochromatin assembly at these repeats may be compromised by parental histone loss during replication. To test this, we analyzed ChOR-seq data to identify genomic regions with decreased H3 occupancy. Compared with non-repetitive regions, repetitive elements exhibited a more pronounced loss of H3, which was also dependent on HU treatment (Figure

2G). Notably, in fork reversal–deficient cells, nearly all classes of repetitive sequences displayed significant reductions in H3 occupancy (Figure 2H). Previous studies have shown that parental histone loss can lead to transcriptional activation of heterochromatic regions. We therefore examined whether histone loss at repeats during replication results in transcriptional derepression. CUT&RUN-seq profiling of the active transcription mark H3K4me3 revealed increased signal both globally and at repetitive elements in FRKO cells (Figure 2I-J). Collectively, these results demonstrate that fork reversal deficiency causes parental histone loss, leading to compromised heterochromatin integrity at repetitive regions.

PrimPol-mediated repriming causes nucleosome density reduction

Next, we sought to understand how fork reversal deficiency leads to low nucleosome density and parental histone loss. Histone chaperones are responsible for histone deposition. We asked if fork reversal deficiency impairs the recruitment of parental histone chaperones to the DNA replication fork. In our proteomic dataset from fork reversal–deficient cells, nearly all known histone chaperones at replication fork were not altered, compared to wild type (Figure 3A), suggesting that the loss of parental histones and reduced nucleosome density were not due to defects in histone recycling.

We noted that PrimPol (Primase And DNA Directed Polymerase) levels at replication forks were elevated after HU treatment in fork reversal–deficient cells (Figure 1A), consistent with previous reports of PrimPol activation under fork reversal defects[63,64,76]. We hypothesized that PrimPol activation contributes to nucleosome density loss. Following HU treatment, fork reversal deficient cells exhibited abundant ssDNA gaps on nascent DNA (Figure 3B, Figure S4B–D), mild DNA damage (Figure S4E–F), and a slight cell cycle arrest in G1 phase (Figure S4G).

To test whether PrimPol activation was responsible for reduced nucleosome density, we depleted PrimPol in FRKO cells by siRNA or CRISPR–Cas9 and measured nucleosome density on nascent DNA by PLA. PrimPol loss rescued nucleosome density reduction (Figure 3C–D, Figure S4G) and restored H3K9me2/3 levels on nascent DNA (Figure 3E–F). To further determine whether nucleosome loss was due to increased PrimPol protein or its catalytic activity, we reintroduced either wild-type PrimPol or a catalytically inactive point mutant (AxA (catalytic dead), CH (primase dead, polymerase competent) mutants) into PrimPol-knockout cells. Only wild-type PrimPol restored the nucleosome density defect, demonstrating that repriming activity itself drives the phenotype (Figure 3G-H). Collectively, these results show that in the absence of fork reversal, activation of the PrimPol-mediated repriming pathway leads to parental histone loss and reduced nucleosome density on nascent DNA.

Single-stranded DNA gaps cause low nucleosome density in cells

Given that PrimPol-mediated repriming produces abundant ssDNA gaps on nascent DNA, we hypothesized that ssDNA gaps themselves inhibits nucleosome assembly (Figure 3I). To test this hypothesis, we examined nucleosome assembly in cells with ssDNA gaps generated through distinct genetic deficiencies.

Firstly, loss of BRCA1 or BRCA2—key fork protection factors—combined with HU treatment led to nucleolytic degradation of nascent DNA, PrimPol activation, and ssDNA gap formation[65,77-81]. In BRCA1- or BRCA2-deficient cells, nucleosome density at replication forks was reduced; however, re-expression of wild-type BRCA1 or BRCA2 rescued the defect (Figure 4A–D, Figure S5A–D). Secondly, defects in Okazaki fragment maturation, such as knockdown of DNA ligase 1 (LIG1) or FEN1 (Flap Endonuclease 1), caused ssDNA gaps on the lagging

strand[81], which also led to reduced nucleosome density (Figure 4F–G, Figure S5E–F). Finally, inhibition of RAD51 triggered nucleolytic degradation of nascent DNA by nucleases such as MRE11, producing ssDNA gaps[80,82]. RAD51 inhibition reduced nucleosome density, and this effect was rescued by co-treatment with MRE11 nuclease inhibitor (Figure 4E, Figure S5G)

Taken together, multiple distinct pathways that generate ssDNA gaps—of various origins—lead to reduced nucleosome density, supporting the hypothesis that ssDNA gaps directly contribute to nucleosome density loss.

Single strand DNA gaps do not block nucleosome assembly in the in vitro assay

Whether nucleosomes can form on ssDNA remains controversial. During DSB resection, the generation of long ssDNA tails/overhangs has been shown to evict nucleosomes in some studies[83-89], whereas others have demonstrated nucleosome formation on ssDNA in vitro[90,91], and ChIP-qPCR analyses in yeast have detected histone association with ssDNA[92]. However, whether short ssDNA gaps, as occur at replication forks, can support nucleosome assembly remains unclear.

We synthesized DNA substrates containing ssDNA gaps either at the dyad (middle), or at the entry/exit (side) of a nucleosome, with various lengths (1–31 nt) and performed in vitro nucleosome assembly assays (Figure 5A-B). We observed nucleosomes on both DNA substrates containing up to a 31-nt gap, although their stability was reduced in dyad-gap substrate (Figure 5B). An AlphaFold model of a nucleosome containing an ssDNA gap is shown in Figure 5C-D. Thus, in vitro, short ssDNA gaps do not preclude nucleosome formation.

PARylation suppresses nucleosome assembly on ssDNA gaps in fork reversal deficient cells

We reasoned that the ssDNA gap metabolism in cells plays a critical role in nucleosome assembly (Figure 4 and Figure 5). In general, the ssDNA intermediates can be either recognized by RPA complex to activate ATR signaling pathway, or bound by PARP1 to stimulate PARylation mediating DNA damage repair. (Phosphorylated) RPA complex accumulated upon HU treatment compared with WT cells (Figure 6A and Figure S4B-E). Nonetheless, depletion of RPA1 and/or RPA2 did not rescue the low nucleosome density in fork reversal-deficient cells (Figure S6B).

PARylation is known to loosen chromatin structure, expose DNA to repair factors, and orchestrate DNA repair[93-99]. We therefore tested whether PARP1-mediated PARylation affects nucleosome density by deleting PARP1 in FRKO cells using siRNA. PARP1 deletion reduced PARylation and partially rescued nucleosome density despite persistent ssDNA gaps (Figure 6B-D). Inhibition of PARG, the enzyme that hydrolyzes PAR chains, increased PARylation and decreased nucleosome density in WT cells, further supporting the conclusion that PARylation reduces nucleosome density (Figure 6E and Figure S6C).

Together, these findings indicate that ssDNA activates PARP1-mediated PARylation, which in turn inhibits nucleosome assembly on nascent DNA.

Interestingly, treatment with the PARP1/2 inhibitor did not rescue the low nucleosome density in FRKO cells (Figure 6F), although the PARylation level was comparable with PARP1 depletion, and the ssDNA gap level remained high (Figure 6D and figure 6G). We also noticed that olaparib treatment in WT cells reduced nucleosome density (Figure 6F), We hypothesized that PARP1 trapping itself can evict nucleosome. This phenotype is consistent with the recent finding

that PARP1 inhibition evict histones from forks, therefore, histone turnover may determine PARP inhibitor sensitivity [100]. We observed FRKO cells were more sensitive to PARP inhibitor, although nucleosome did not further decrease. The hypersensitivity to PARPi in FRKO cells may be caused by excessive ssDNA gaps.

HMCES–DPC inhibits nucleosome assembly on ssDNA

Since PARP1 deletion only partially rescued the reduction in nucleosome density, we sought additional factors that might bind ssDNA and inhibit nucleosome assembly. We noted that in fork reversal–deficient cells, APOBEC3B levels at replication forks increased by ~1.5-fold (Figure 7A), chromatin-bound APOBEC3B increased by 3–5-fold (Figure S6I), and HMCES showed a modest increase (Figure 7A). APOBEC3B can deaminate cytosine residues, which are subsequently processed by glycosylases to generate AP sites[101]. HMCES, a PCNA-binding protein, has been shown to form covalent DNA–protein crosslinks (DPCs) at AP sites on ssDNA[102-108].

We hypothesized that in fork reversal–deficient cells, the high abundance of ssDNA on nascent DNA permits excess APOBEC3B activity, leading to the generation of AP sites that subsequently form HMCES–DPCs. These DPCs may create steric hindrance that blocks nucleosome assembly. To test this, we performed a RADAR assay to examine HMCES–DPCs in fork reversal–deficient cells and found that HMCES–DPCs were significantly increased in FRKO cells (Figure 7B). We then depleted HMCES or APOBEC3B using siRNA and measured nucleosome density on nascent DNA by PLA (Figure 7C, Figure S7B–C). HMCES depletion significantly restored nucleosome density in fork reversal–deficient cells, whereas APOBEC3B depletion did not (Figure 7C), likely because AP sites can also form spontaneously on ssDNA

independent of APOBEC3B. Co-deletion of PARP1 and HMCES completely rescued nucleosome density in fork reversal–deficient cells (Figure 7D). HMCES loss is also known to activate TLS (translesion synthesis) for post-replication repair[103], which in turn repair ssDNA gaps[65,76]. We next asked whether the rescue of nucleosome density upon HMCES depletion was mediated by TLS-dependent gap repair. Inhibition of TLS using the REV1 inhibitor JH-RE-06 in HMCES-deficient cells did not reduce nucleosome density (Figure 7E), demonstrating that HMCES–DPCs themselves, rather than TLS activation, block nucleosome assembly.

To further validate whether HMCES–DPCs directly block nucleosome assembly, we performed an in vitro nucleosome assembly assay. We synthesized ssDNA substrates containing gaps with uracil either at the center (APDyad) or near the end (APend), treated them with UNG, and then induced HMCES crosslinking[103,104](Figure S7D-E).

After purification, these substrates were used for nucleosome assembly. Strikingly, nucleosomes could not form on substrates containing an HMCES–DPC at the dyad position (Figure 7F), whereas nucleosomes could still assemble on substrates with HMCES–DPCs at end gaps (Figure 7G). These data indicate that HMCES–DPCs formed at interstitial ssDNA gaps, but not at end gaps, directly impair nucleosome assembly.

Together, these findings demonstrate that in FRKO cells, PrimPol-mediated repriming generates abundant ssDNA gaps, which activate PARP1-dependent PARylation and promote HMCES–DPC formation. At least two mechanisms—PARylation and HMCES–DPC formation—act in concert to inhibit nucleosome assembly on ssDNA gaps, thereby reducing parental histone recycling and lowering nucleosome density on nascent DNA (Figure 7H).

Discussion

A mechanistic model for fork reversal–dependent epigenetic stability

Under persistent replication stress, replication forks are not completely stalled but exist in a dynamic equilibrium between repair and restart, progressing slowly yet continuously[109]. Stalled replication forks can be resolved through fork reversal, PrimPol-mediated repriming, or DNA damage tolerance pathways. Previous studies of parental histone recycling have largely focused on unperturbed forks; whether and how fork resolution pathways coordinate nucleosome assembly under replication stress has remained unclear.

Here, we uncover a critical role for fork reversal in maintaining epigenetic stability during stressed replication. We propose a new mechanistic model: under replication stress, fork reversal suppresses ssDNA gap formation, thereby promoting parental histone recycling and nucleosome assembly on nascent DNA, preserving the epigenetic state of chromatin. In the absence of fork reversal, PrimPol-mediated repriming generates abundant ssDNA gaps, which activate PARP1-dependent PARylation and induce HMCES–DPC formation. These events subsequently inhibit nucleosome deposition and lead to loss of parental histone modifications (Figure S4A, Figure 5G). Thus, fork reversal safeguards both genome and epigenome stability under replication stress.

Parental histone and epigenetic information are lost in fork reversal deficient cells

Previous studies identified H3K9me3 and other marks (H4K20me2, H3K79me2, H3K27me3) as parental-histone modifications at replication forks. By iPOND-MS (Figure 2), these parental-histone-specific marks decreased in FRKO cells, whereas new-histone marks (H3K9ac, H4K5ac,

H3K56ac, H4K12ac) were unchanged or slightly increased (Figure 2B). PLA assays corroborated these findings. Additionally, histone variants MacroH2A.1, MacroH2A.2, H3.3, and CENPA are not incorporated during replication and thus derive exclusively from parental chromatin[71-73];

Their loss in FRKO cells (Figure 1A) provides direct evidence of parental-histone depletion. Altogether, these results indicate that fork reversal is required to maintain parental histones during replication under stress.

Loss of parental histones subsequently leads to epigenetic alteration and transcriptional dysregulation, since canonical parental-histone marks (H4K20me2, H3K9me3, H3K27me3) promote chromatin compaction and repress transcription. More than half of the genome comprises repetitive DNA elements, including transposons and retrotransposons, that rely on these heterochromatin marks for silencing. Consequently, parental-histone loss can activate transcription of repetitive elements, thereby threatening genome stability. Indeed, ChOR-seq analysis of H3-depleted regions revealed reduced nucleosome density at repetitive regions during replication (Figure 2). CUT&RUN-seq mapping of steady-state H3K4me3 showed increased signal at many repetitive-element promoters, suggesting their activation (Figure 2). Collectively, our work explains how fork reversal preserves both genome and epigenome stability and highlights repetitive, replication-challenged regions as particularly vulnerable to epigenetic information loss in the absence of fork reversal.

Fork-reversal deficiency selectively impairs parental-, but not new-, histone assembly

We next asked whether fork-reversal enzymes function as histone chaperones required for parental-histone recycling, while deposition of new histones might proceed independently of them. We found that known histone chaperones were properly recruited to replication forks in FRKO cells (Figure 3A), indicating that fork-reversal enzymes do not control chaperone recruitment. However, co-depletion of PrimPol in FRKO cells rescued parental-histone loss on nascent DNA (Figure 3), suggesting that PrimPol-mediated ssDNA gap formation—rather than loss of fork-reversal enzymes per se—drives parental-histone depletion. Consistently, accumulation of ssDNA gaps caused by BRCA1/2 deficiency, failure of Okazaki fragment processing, RAD51 knockdown, or MRE11 inhibition also resulted in parental-histone loss. Conversely, reintroduction of BRCA1/2 into deficient cells restored parental-histone deposition at replication forks (Figure 4, Figure S5).

Our data support a model in which, in fork-reversal–deficient cells, parental histones bound to ssDNA are unstable and evicted (Figure 3–5). As ssDNA gaps are gradually repaired to generate dsDNA post-replication, re-chromatinization occurs after parental histone loss, with new histones deposited onto the repaired forks (Figure 2). Several observations support this model: (1) nucleosomes can assemble on ssDNA gaps but are unstable and subject to eviction under conditions such as BRCA1/2 deficiency, HMCES–DPC formation (both in vitro and in vivo), PARylation, and in vitro nucleosome-assembly assays on ssDNA gaps; and (2) ssDNA gaps are gradually repaired—by homologous recombination (HR) during S phase and/or by TLS in G2 phase. In our studies, RAD51 depletion or inhibition (blocking HR repair; Figure 1C, Figure 4F) further reduced nucleosome density in fork-reversal–deficient cells (Figure 3C and ref.), whereas TLS inhibition had no effect (Figure 3D), indicating that ongoing ssDNA repair primarily involves HR under HU treatment, which arrests cells in S phase.

Fork reversal is essential for both genome stability and epigenome stability

DNA replication must preserve both genome and epigenome stability. Fork reversal enables cells to maintain this integrity under replication stress. In the absence of fork reversal, PrimPol-mediated repriming allows replication restart downstream of DNA lesions, completing DNA synthesis but at the cost of generating abundant ssDNA gaps on nascent DNA. These gaps can be repaired post-replication (Figure 3). However, the loss of parental histones compromises gene regulation in daughter cells, since rebuilding heterochromatin relies on inherited parental marks such as H3K9me3. As a result, repetitive elements such as LINE-1 are derepressed when parental histones are lost. Co-inhibition of repriming in fork-reversal–deficient cells reduces ssDNA gap formation and slows replication, thereby permitting parental-histone recycling but increasing sensitivity to replication stress (Figure 3, Figure S4). We propose that the physiological function of fork reversal is not only to safeguard genome stability but also to maintain epigenome stability under replication stress.

Limitations and future directions

Although our study identifies a key role for fork reversal in regulating epigenetic stability, several important questions remain. First, the fate of parental histones during fork reversal. It remains unclear whether parental nucleosomes ahead of the fork are directly recycled onto the reversed arm, released into a free pool, or repositioned via a “sliding” mechanism. Current technology does not allow real-time spatial tracking of nucleosomes during fork reversal, limiting mechanistic insight. Second, the relationship between PARylation and HMCES–DPCs. Whether these are independent, cooperative, sequential, or feedback-regulated pathways is unknown. Additional ssDNA-binding proteins may also act with HMCES to sterically hinder

nucleosome assembly. Third, the extent of compensation by new histone deposition. Although new-histone marks (e.g., H3K56ac) increased in response to parental-histone loss, whether this quantitatively restores nucleosome density remains uncertain. Our data suggest incomplete compensation, possibly due to the absence of compaction-associated marks such as H3K9me3. Fourth, epigenetic restoration post-replication. Despite loss of parental marks on nascent DNA, global H3K9me2/3 levels were unchanged, suggesting the existence of post-replicative "epigenetic repair" mechanisms. Whether this restoration occurs in a locus-specific manner remains unknown and has implications for whether epigenetic stability is truly preserved. Fifth, feedback effects on replication fork stability. Some histone modifications lost in fork-reversal–deficient cells, such as H3K9me2/3 and H4K20me3, also contribute directly to fork protection. Whether their loss further destabilizes forks and exacerbates replication stress remains to be determined. Addressing these questions will require integrating high-resolution chromatin mapping, single-molecule localization, quantitative proteomics, and in situ functional assays to fully elucidate chromatin dynamics under replication stress.

Materials and **Methods**

Cell lines

U2OS and MDA-MB-436 cells were cultured in DMEM with 9% fetal bovine serum (FBS)corning. PEO4, PEO1, and DLD-1 cells were cultured in RPMI-1640 with 9% fetal bovine serum (FBS). UWB1.289 cells were cultured in a 1:1 mixture of RPMI-1640 medium and Mammary Epithelial Growth Medium (MEGM), supplemented with fetal bovine serum (FBS) and antibiotics. U2OS cells for iPOND mass spectrometry experiments were cultured in SILAC-compatible DMEM (Thermo) + 10% dialyzed FBS (Thermo Fisher Scientific, catalog no.

A33822; R&D Systems, catalog no. S12850H), supplemented with either isotopically light or heavy 13C, 15N lysine, and 13C,15N arginine (Cambridge Isotope Laboratories)[109]. Cells were cultured at 37°C and 5% CO2 with humidity. All cell lines were regularly tested for mycoplasma and verified using short tandem repeat profiling.

Genome editing

PrimPol knockout by CRISPR-Cas9 using the SpCas9(BB)-2A-Puro (PX459) V2.0 plasmid (Addgene #62988) as described[110] with single guide RNA (sgRNA) #1 (5'-CTGCCAAGCAAGTCAAGAGC-3'),

Label free iPOND-mass spectrometry

Proteomics changes in U2OS cells were determined using iPOND-SILAC MS as described previously[109]. Briefly, EdU labeled and indicated drug treated cells were harvested following cross-linking with 1% formaldehyde for 10 min and quenched with glycine. Cells were permeabilized in 0.25% Triton X-100/PBS for 30 min. Heavy labeled and light labeled cells were combined 1:1 prior to performing the click reaction for 2 hrs. Dynabeads MyOne Streptavidin C1 (Thermo Fisher, Cat# 65002) were utilized to capture DNA-protein complexes, washed, and elute with elution buffer (25mM biotin, 0.4% SDS, 50mM Tris-HCl Ph8.5) at 65°C for 3 hrs. Supernatant, containing eluted fractions, were incubated at 95°C for 10 mins for reverse crosslinking. For histone modification detection, lysine residues were chemically modified by propionylation for 30 min at room temperature with 2.5% propionic anhydride (Sigma-Aldrich, 8.00608) in ammonium bicarbonate (pH 7.5). Subsequently, proteins were digested with 200 ng of trypsin (Thermo Fisher, 90057) in 50 mM ammonium bicarbonate

overnight, and the supernatant was desalted by C18 Stagetips (reversed-phase resin) and carbon Top-Tips (Glygen, TT1CAR) according to the manufacturer's instructions. After desalting, the eluent was speed-vacuumed dried and stored at −20°C until MS analysis.

PrimPol complementation

PrimPol WT, AxA, and CH mutants are subcloned from pcDNA3.1/nV5-DEST to pLNCX2 with forward primer: 5'-CAGATCTCGAGATGAATAGAAAATGGGAAGCAA-3', reverse primer: 5'-CTGCGGCCGCCTCTTGTAATACTTCTATAATTAG-3'. pLNCX2-Primpol WT and mutants vectors were co-transfected with p-VSVG into GP2-293 cells with Polyethylenimine (PEI). Twenty-four hours post-transfection, the culture medium was replaced with fresh medium, and viral supernatants were harvested at 48 and 72 hours. The pooled viral supernatants were subsequently used to infect U2OS Primpol knockout #206 cells. Stable cell lines were established by selection with 100 μg/ml G418.

DNA combing assays

Cells were labeled with the nucleoside analogs as indicated in the figures and figure legends. DNA combing was then performed using a DNA combing instrument as previously described[52]. The S1 nuclease digestion assay was also completed as previously described[64].

Immunofluorescence

For analysis of proteins in the insoluble/chromatin fraction, cells were detergent extracted with 0.5% Triton X-100 and subsequently fixed in 4% paraformaldehyde. Slides were blocked with 1% goat serum in PBST (0.1% triton-X100) and incubated with primary antibodies. EdU

incorporation was visualized by click chemistry with an Alexa Fluor 488-conjugated azide. Immunofluorescent images were obtained and analyzed by ImageXpress microscopy and software.

PLA assay

Proximity ligation assays (PLAs) were performed using the Sigma kit (Duolink DUO92002, DUO92004, DUO92008) according to the manufacturer's instructions, with the following modifications as described previously [111]. Cells were pre-extracted and fixed as described in the immunofluorescence method, then blocked with 3% BSA and processed via click chemistry with biotin-azide and Alexa Fluor 488-conjugated azide (ratio 4:1). The following primary antibody pairs were used: rabbit H2A (CST 12349) (1:100 dilution), H3 (Abcam ab1791) (1:100 dilution), H3K9ac (Millipore 07-352) (1:100 dilution), H3K9me3 (CST 13969) (1:100 dilution), H4 (CST 13919) (1:100 dilution); mouse biotin (Millipore B7653) (1:100 dilution) and mouse H2B (Abcam ab52484) (1:100 dilution), H3K9me2 (Abcam ab1220) (1:100dilution) and rabbit biotin (CST 5597) (1:100 dilution).

CHOR-Seq

ChoR-seq assay performed as previous described[70]. ChOR-seq assay was performed on wild-type (WT) and triple-knockout (3KO) U2OS cells (three biological replicates each) to characterize histone H3 on nascent DNA following previous described (reference). In briefly, cells were labeled with 10 uM EdU for 15 min, followed by treatment with or without 1 mM hydroxyurea (Sigma, Cat. no. H8627) for 4 h. Cells were then fixed in fixation buffer A (truChIP Chromatin Shearing Kit, Covaris, Cat. No. 520127), and 11.1% formaldehyde was added to a

final concentration of 1% for 10 min with gentle agitation at room temperature. The reaction was quenched by adding buffer E for 5 min. Fixed cells were washed twice in ice-cold PBS and then collected for 5 min at 500 g at 4 °C, snap-frozen, and stored at −80 °C or processed immediately. Nuclei were isolated using truChIP Chromatin Shearing Kit according to the instruction and sonicated chromatin fragments between 100 and 500 bp. Sheared chromatin was centrifuged at 14,000 rpm at 4 °C for 10 min, and the supernatant was collected for subsequent steps. In parallel, Drosophila S2 cells were labeled with 10 μM EdU for 48 h, fixed, lysed, and sonicated identically. EdU-labeled S2 chromatin was added to each sample after sonication at 0.05% (w/w) as a spike-in for cross-sample normalization. For each ChIP, 100 μg mixed chromatin were diluted up to 500 μl with dialysis buffer [4% glycerol, 10 mM tris-HCl, 1 mM EDTA, and 0.5 mM EGTA (pH 8)] and 400 μl of incubation buffer [2.5% Triton X-100, 0.25% sodium deoxycholate, 0.25% SDS, 0.35 M NaCl, and 10 mM tris-HCl (pH 8)] supplemented with leupeptin, aprotinin, and phenylmethylsulfonyl fluoride (PMSF). Chromatin was precleared with Protein A/G Magnetic Beads (Thermo Fisher Scientific, Cat. no. 88803) for 1 h at 4°C and then incubated with 10 ug H3 antibody (Abcam, Cat. no. ab1791) overnight at 4 °C. The following day, the mix was captured 3 h at 4°C with pre-blocked Protein A/G Magnetic Beads [incubated in BSA (1 mg/ml) in RIPA buffer overnight]. Subsequently, beads were washed three times in ice-cold RIPA buffer [140 mM NaCl, 10 mM tris-HCl, 1 mM EDTA, 1% Triton X-100, 0.1% SDS, and 0.1% sodium deoxycholate (pH 8)], three times in high-salt RIPA buffer (0.5 M NaCl), once in LiCl buffer [250 mM LiCl, 10 mM tris-HCl, 1 mM EDTA, 0.5% IGEPAL CA-630, and 0.5% sodium deoxycholate (pH 8)], and twice in TE buffer [10 mM tris-HCl and 1 mM EDTA (pH 8)]. The washed beads were resuspended with 100 μl TE buffer, transferred to a PCR tube, added 5 μl RNase A (New England Biolabs, Cat. No. T3018L), and incubated for 1 h at 37 °C.

Thereafter, SDS and NaCl were added to a final concentration of 0.5% and 100 mM, respectively, and samples were incubated with 10 ug proteinase K (Research Products International, Cat. no. P50220) for 10 h at 37 °C followed by 6 h incubation at 65 °C for decross-linking. DNA was purified using the MinElute PCR purification kit (QIAGEN, Cat. No. 28004). All immunoprecipitated DNA subjected to end repair, A-tailing, and adaptor ligation using the NEBNext® Ultra™ II DNA Library Prep Kit (New England Biolabs, Cat.no. E7645S) following the manufacturer's instructions and cleaned up with AMPure XP beads (Beckman Coulter, Cat. no. B23318). Then, Click-iT was performed on indexed DNA for 1 h at room temperature under the following conditions: 10 × PBS, 0.5 mM picolyl-azide-PEG4-biotin (Sigma, Cat. no. CHM02H272), 0.5 mM Tris(3-hydroxypropyltriazolylmethyl)amine (THPTA) (Sigma-Aldrich, Cat. no. 762342), 0.1 mM CuSO4, and 10 mM sodium ascorbate (Sigma, Cat. no. A4034). DNA fragments between 200 and 700 bp were size-selected using AMPure XP beads and resuspended in TE buffer. Next, to capture biotinylated products, 10 ul MyOne Streptavidin T1 beads (Invitrogen, Cat. no. 65602) were washed three times with 1 × BWT buffer [5 mM tris-HCl (pH 7.5), 0.5 mM EDTA, 1 M NaCl, and 0.05% (v/v) Tween 20] and resuspended in 2 × BWT buffer at a volume equal to the volume of biotinylated DNA. Streptavidin beads were then mixed with biotinylated DNA and rotated at 20 rpm for 2 h at room temperature. Beads containing biotinylated DNA were washed four times with 1 × BWT buffer, twice with 1 × EBT buffer [10 mM tris-HCl (pH 8.5) and 0.05% (v/v) Tween 20]. Last, beads were resuspended in double distilled water. PCR amplification was performed following the NEBNext® Ultra™ II DNA Library Prep Kit protocol using the streptavidin bead suspension as a template (11 cycles of PCR). Following PCR, streptavidin beads were purified using a magnet, and the supernatant was cleaned up with AMPure XP beads at a ratio of 0.8 ×. Fragment distribution of libraries was

checked using the Fragment Analyzer system (Agilent - Tape Station - DNA5000 HS kit), libraries were pooled and sequenced paired-end on NovaSeq X Plus Series.

Radar Assay

Cells were lysed in Radar buffer (4M Guanidine thiocyanate, 1% Sarkosyl, 2% Triton X-100, 1% 1,4-dithioerythritol, 100 mM Sodium Acetate pH5.0, 20 mM Tris pH 8.0, 20 mM EDTA pH8.0; adjusted to pH 6.5). Genomic DNA was sonicated and precipitated with ethanol, resuspended in 8 mM NaOH, and quantified using Qbit fluorometry. Samples were then subjected to slot-blot onto nitrocellulose membrane??, which were subsequently immunoblotted with HMCES primary antibody and corresponding secondary antibody. ibody and corresponding secondary antibody.)

RNA interference

All siRNA transfections were performed using DharmaFECT reagents according to the manufacturer's instructions. Experiments were performed 2 days after transfection. See table for siRNA sequences. Qiagen AllStars Negative Control Nontargeting (NT) siRNA was used in samples where a gene-selective siRNA is not indicated or to bring the total amount of siRNA to equal molar concentrations when comparing samples with one versus two siRNAs.

HMCES purification

HMCES protein purification using a protocol as described previously[112]. Briefly, pNIC-HMCES vector was transformed in *E. coli* cells. Cells were grown in terrific broth (TB) medium at 37°C till OD600 reached 0.7. Protein expression was induced by addition of 0.5 mM isopropyl- β-D-

thiogalactoside (IPTG) for 4 hrs. Cell pellets were collected and resuspended in buffer A (20 mM HEPES/KOH pH 7.5, 500 mM KCl, 5 mM $MgCl_2$, 30 mM imidazole, 10% glycerol, 0.1% IGEPAL, 0.04 mg/ml Pefabloc SC, cOmplete EDTA-free protease inhibitor cocktail, and 1 mM TCEP). Wash steps used buffer B (20 mM HEPES/KOH pH 7.5, 500 mM KCl, 5 mM $MgCl_2$, 1 mM TCEP). Protein was eluted from Strep-Tactin® XT Superflow® high-capacity cartridges with buffer B supplemented with 50 mM biotin, and from HiTrap Heparin HP columns with buffer C (20 mM HEPES/KOH pH 7.5, 1 M KCl, 5 mM $MgCl_2$, 1 mM TCEP). Size-exclusion chromatography and protein storage were carried out in buffer D (20 mM HEPES/KOH pH 7.8, 150 mM KCl, 5 mM $MgCl_2$, 10% glycerol, 1 mM TCEP).

Quantification and statistical analysis

The statistical test was performed using GraphPad Prism and R software. The statistics for the high-content microscopy experiments was performed on the mean of individual replicates. Statistical analyses were completed using Prism. A Kruskal-Wallis test was used for experiments with more than two samples, and P values were calculated by Prism for the multiple comparisons. A two-tailed t test was used to compare two samples with normally distributed data. No statistical methods or criteria were used to estimate sample size or to include/exclude samples. Statistical details of individual experiments can be found in the figure legends and in Results. Experiments shown are representative of at least two biological replicates unless otherwise indicated in the figure legend.

Acknowledgement:

We would like to thank David Cortez Lab for the SMARCAL1, HLTF, ZRANB3 single and triple knockout U2OS cell lines. Alessandro Vindigni lab for the pcDNA3.1/nV5-DEST PrimPol

WT and Mutants vectors; Sharon Cantor lab for the FANCJ KO cell lines, and FANCJ WT vectors; Weixing Zhao lab for the MDA-MB-436 and BRCA1 complemental cell lines, DLD-1 WT and BRCA2 knockout cell lines.

Author contribution:

W.L. conceptualized the project. Q.W. and C.Z. performed PLA, IF, iPOND, western blot assays. Y.D. and T.Z. performed Mass spectrometry experiments. N.I.M and T.M.W performed in vitro nucleosome assembly assays. M.G. and S.T. purified HMCES proteins and performed RADAR assay. W.L. and Q.W. wrote the manuscript with contributions from all the authors.

Figure Legend

Figure 1. Fork reversal deficiency reduces nucleosome density on nascent DNA

A) iPOND-SILAC-MS analysis of proteins bound to nascent DNA in HU-treated wild-type (WT) and fork reversal enzyme knockout (FRKO) U2OS cells. WT and FRKO cells were labeled with light and heavy isotopes for ⩾4 weeks, pulse-labeled with EdU and treated with 1mM HU for 4 h prior to iPOND. N = 4 biological replicates; error bars represent SD.

B–D) PLA for EdU and H3 in WT or FRKO cells labeled with 10 μM EdU and treated with 1 mM HU. B) Representative images (Texas Red = PLA signal; green = EdU). C) PLA foci per cell; each dot represents a single cell. D) PLA signal normalized to EdU intensity. ⩾1,000 cells/sample were analyzed with MetaXpress (Molecular Devices). N ⩾ 10. p-values from two-tailed unpaired t-test.

E) Heatmaps of H3 ChOR-seq signal in WT and FRKO cells treated with HU, normalized to spike-in chromatin from D. melanogaster S2 cells. N = 2.

F–G) Genome browser views of H3 ChOR-seq from the same experiment in (E), normalized to reads per million using exogenous spike-in. N = 2.

H) PLA for EdU and H3 in WT or FRKO cells with siRAD51 knockdown. N = 3. p-values from Kruskal–Wallis test.

Figure 2 Fork reversal deficiency leads to parental histone loss on nascent DNA

A) Schematic of iPOND–propionylation-MS workflow to detect histone modifications on nascent DNA in WT and FRKO U2OS cells treated with EdU together with 1mM HU for 4 h.

B) Log_2 fold-change of histone modifications in FRKO vs. WT cells. Modification-specific peptide counts were normalized to unique peptide numbers, and FRKO/WT ratios plotted on log_2 scale. N = 3.

C) PLA for EdU and H3K9me3 in WT and FRKO cells treated as in (A). PLA signals normalized to EdU intensity. ⩾1,000 cells/sample. N = 3. p-values from two-tailed unpaired t-test.

D–E) Immunofluorescence for H3K9me3 in S-phase WT and FRKO cells. D) Cells pulse-labeled with EdU (10 min). E) Cells labeled with EdU and treated with HU (4 h). Quantification by QIBC. N = 3.

F) PLA for EdU and H3K9me2 in WT and FRKO cells treated as in (A). PLA signals normalized to EdU intensity. ⩾1,000 cells/sample. N = 3.

G) ChOR-seq analysis of H3 occupancy categorized into total genome, non-repeats, and repeats, in WT and FRKO cells under HU or no-HU conditions. Signal normalized using D. melanogaster spike-in chromatin. N = 2. p-values from unpaired t-test.

H) H3 ChOR-seq signal at specific repeat classes in WT and FRKO cells under HU. Error bars = SD of two replicates; $p < 10^{-4}$ by paired t-test.

I) Average CUT&RUN profiles of H3K4me3 in WT and FRKO cells across all promoters. Signal normalized to spike-in chromatin. N = 2.

J) CUT&RUN analysis of H3K4me3 enrichment at repetitive elements in WT and FRKO cells. Error bars = SD of two replicates; $p < 10^{-4}$ by paired t-test.

Figure 3 PrimPol deletion rescues low nucleosome density

A) iPOND-SILAC-MS analysis of histone chaperones on nascent DNA (data from Figure 1A). N = 4, error bars = SD.

B) S1 nuclease-treated DNA fiber assay to detect ssDNA gaps. N = 3. p-values from Kruskal–Wallis test.

C–G) PLA for EdU and histone marks in indicated conditions. C–E) H3; F) H3K9me2; G) H3K9me3. PLA signals normalized to EdU intensity; ⩾1,000 cells/sample. N ⩾ 3. p-values from Kruskal–Wallis test.

H) Western blot for PrimPol in KO and complemented cells.

I) Model schematic.

Figure 4. Single-stranded DNA gaps reduce nucleosome density on nascent DNA in cells

A–E) PLA for EdU and H3 in the indicated cell lines and treatments. PLA signals normalized to EdU intensity; ⩾1,000 cells/sample. N ⩾ 3. p-values from Kruskal–Wallis test.

Figure 5. Nucleosomes can assemble on ssDNA-gapped substrates with reduced stability in vitro

A–B) Nucleosome reconstitution assays using DNA substrates containing ssDNA gaps at the dyad (A) or entry/exit site (B). Gaps of varying sizes were tested. Gels show nucleosome core particle (NCP) formation; quantification shown below.

C–D) Structural models of ssDNA-gapped nucleosomes predicted by AlphaFold. C) ssDNA gap at dyad. D) ssDNA gap at entry/exit.

Figure 6. PARylation reduces nucleosome density in fork reversal–deficient cells

A) Immunofluorescence of PARylation in WT and FRKO cells. Cells were labeled with EdU (10 min, no HU) or EdU + HU (4 h). Integrated PARylation intensity quantified. N = 3. p-values from Kruskal–Wallis test.

B) PLA for EdU and H3 under indicated conditions. PLA normalized to EdU intensity; ⩾1,000 cells/sample. N = 9. p-values from Kruskal–Wallis test.

C) Immunofluorescence of PARylation in indicated conditions. N = 3.

D) S1 nuclease DNA fiber assay to detect ssDNA gaps. N = 3. p-values from Kruskal–Wallis test.

E–F) PLA for EdU and H3 in indicated conditions, quantified as in (B). N ⩾ 7.

G) Immunofluorescence for PARylation in the indicated conditions. N = 3.

Figure 7. HMCES-DPC at ssDNA gaps reduces nucleosome density in fork reversal–deficient cells

A) APOBEC3B and HMCES levels on nascent DNA measured by iPOND-SILAC-MS. N = 4.

B) RADAR assay detecting HMCES-DPC in WT and FRKO cells. N = 3.

C–E) PLA for EdU and H3 in indicated conditions (as in Figure 1B). N ⩾ 7. p-values from Kruskal–Wallis test.

F–G) Nucleosome reconstitution assays showing nucleosomes fail to form on dyad ssDNA gaps but can form at side gaps. Gels show NCP bands. AP-DNA = abasic-site DNA; AP-NCP = nucleosomes assembled on abasic DNA. L = ladder, D = DNA, N = nucleosome.

H) Model schematic of how ssDNA adducts interfere with nucleosome formation at gaps.

Supplementary Figure Legends

Figure S1. Fork reversal deficiency reduces nucleosome density on nascent DNA (related to Figure 1).

A) EdU incorporation in WT and FRKO cells treated with EdU + HU (as in Fig. 1B). EdU detected by azide–488 click reaction.

B–E) Immunofluorescence for H3 in WT and FRKO cells under indicated conditions. N = 3; p-values from two-tailed unpaired t-test.

F) PLA for EdU and H3 at different HU concentrations. N = 3; p-values from Kruskal–Wallis test.

G–I) PLA for EdU and H2A (G), H2B (H), and H4 (I). Left: PLA foci/cell; middle: EdU intensity; right: normalized PLA/EdU. $\geqslant$1,000 cells/sample. N $\geqslant$ 3.

J) Quantitative ChOR-seq for H3. Average profiles across H3 peaks in WT and FRKO cells, normalized by reference-adjusted RPM using D. melanogaster spike-in. N = 2; Wilcoxon signed-rank test.

Figure S2. Low nucleosome density is due to fork reversal deficiency, not depletion of individual fork reversal enzymes (related to Figure 1).

A–B) PLA for EdU and H3 in individual fork reversal enzyme KO cells. N = 3.

C) Western blot showing siRAD51 knockdown efficiency.

D) PLA for EdU and H3 in WT and FRKO cells without HU. Cells labeled with EdU (10 min) and harvested for PLA. N = 3; p-values from unpaired t-test.

E) ChOR-seq analysis of H3 occupancy in WT and FRKO cells without HU, normalized to spike-in chromatin.

F) Heatmaps of H3 ChOR-seq signal (from E). N = 2.

G) Model schematic: fork reversal prevents nucleosome loss under replication stress.

Figure S3. Fork reversal deficiency leads to parental histone loss (related to Figure 2).

A–K) Histone modifications quantified in WT and FRKO cells by iPOND–propionylation-MS. Modification level = modified peptide count/unique peptide count. N = 3; error bars = SD.

L) PLA for EdU and H3K9ac in WT and FRKO cells, treated as in Fig. 1B. Signals normalized to EdU. N = 3.

M–R) Immunofluorescence for H3K9me2 and H3K9me3 in indicated conditions. N = 3; unpaired t-test.

Figure S4. Fork reversal deficiency leads to PrimPol-mediated ssDNA gaps and DNA damage (related to Figure 3).

A) S1 nuclease DNA fiber assay detecting ssDNA gaps. N = 3; Kruskal–Wallis test.

B) Native IdU immunofluorescence for parental ssDNA detection. U2OS cells labeled with IdU (50 μM, 48 h), then chased 2 h in fresh medium and treated with HU (1 mM, 4 h). IdU stained without denaturation. N = 3.

C–E) Immunofluorescence for RPA2 (C), RPA2-S8 phosphorylation (D), and γH2AX-S139 (E). N = 3.

F) QIBC for cell cycle analysis.

G) Western blot for PrimPol knockdown efficiency.

Figure S5. Single-stranded DNA gaps inhibit nucleosome assembly in cells (related to Figure 4).

A–G) PLA for EdU and H3 in indicated treatments. PLA foci/cell and EdU intensity shown (same data as Fig. 4). N = 3; p-values from unpaired t-test.

Figure S6. PARylation and HMCES-DPC at ssDNA gaps inhibit nucleosome assembly in FRKO cells (related to Figures 6).

A) Model schematic.

B) PLA for EdU and H3 in siRPA1 and/or siRPA2 cells (treated as in Fig. 1B). N ⩾ 5; Kruskal–Wallis test.

C) Immunofluorescence for PARylation. N = 3.

D) Survival assay in olaparib. 100 WT or FRKO cells plated per 10-cm dish, treated with indicated olaparib concentrations 24 h post-plating, and maintained for 10 d.

Figure S7. HMCES-DPC at ssDNA gaps reduces nucleosome density in FRKO cells (related to Figure 7).

A) Western blot for chromatin-bound APOBEC3B in WT and FRKO cells ± HU.

B–C) Western blot for HMCES (B) and APOBEC3B (C) to confirm knockdown efficiency in WT and FRKO cells.

D-E) HMCES-ssDNA crosslink preparation. Gels show HMCES–DNA crosslink products. AP-DNA = abasic DNA; L = ladder.

Figure 1 Fork reversal deficiency reduces the nucleosome density on nascent DNA

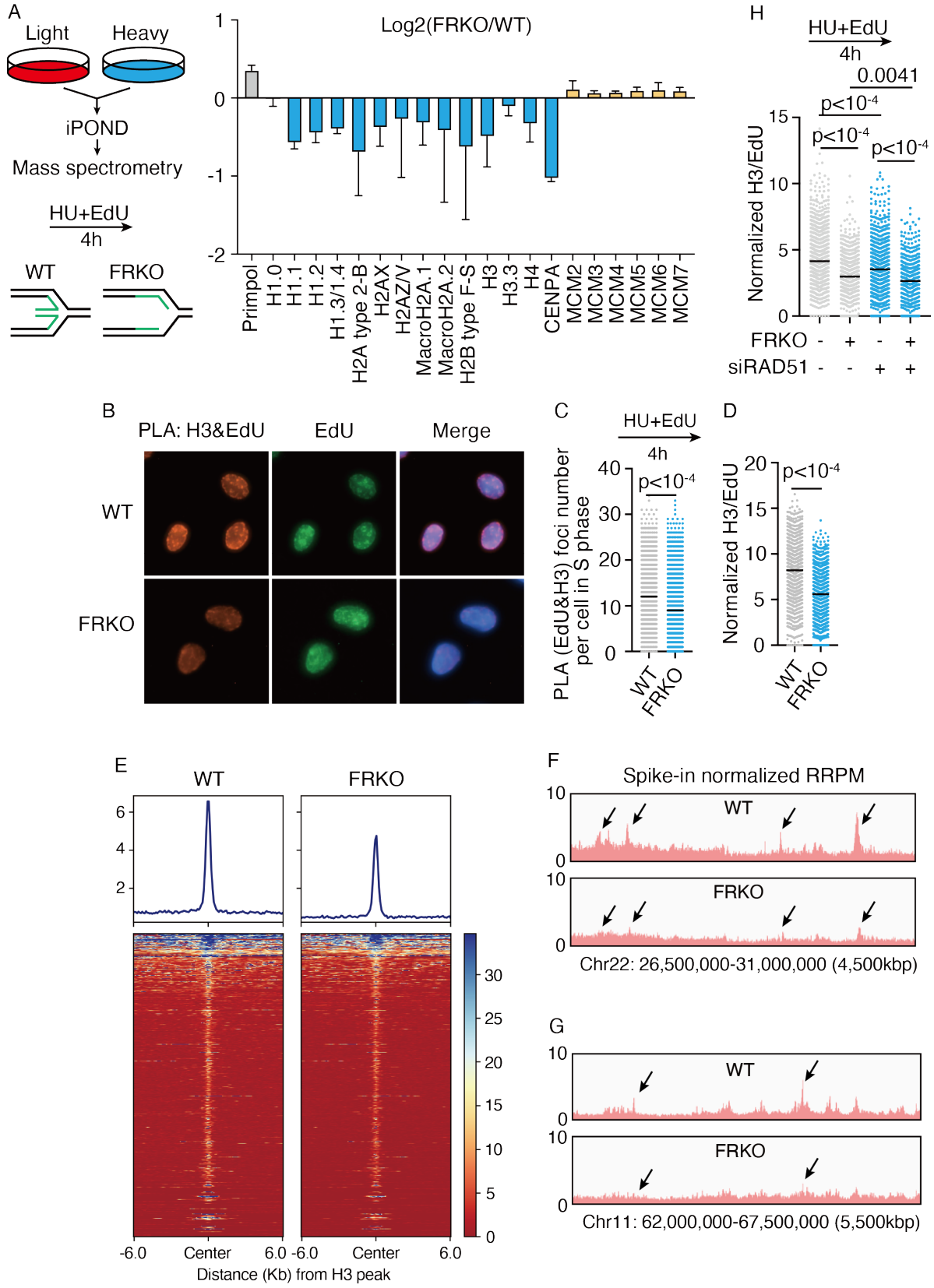

Figure 2 Fork reversal deficiency leads to parental histone loss on nascent DNA

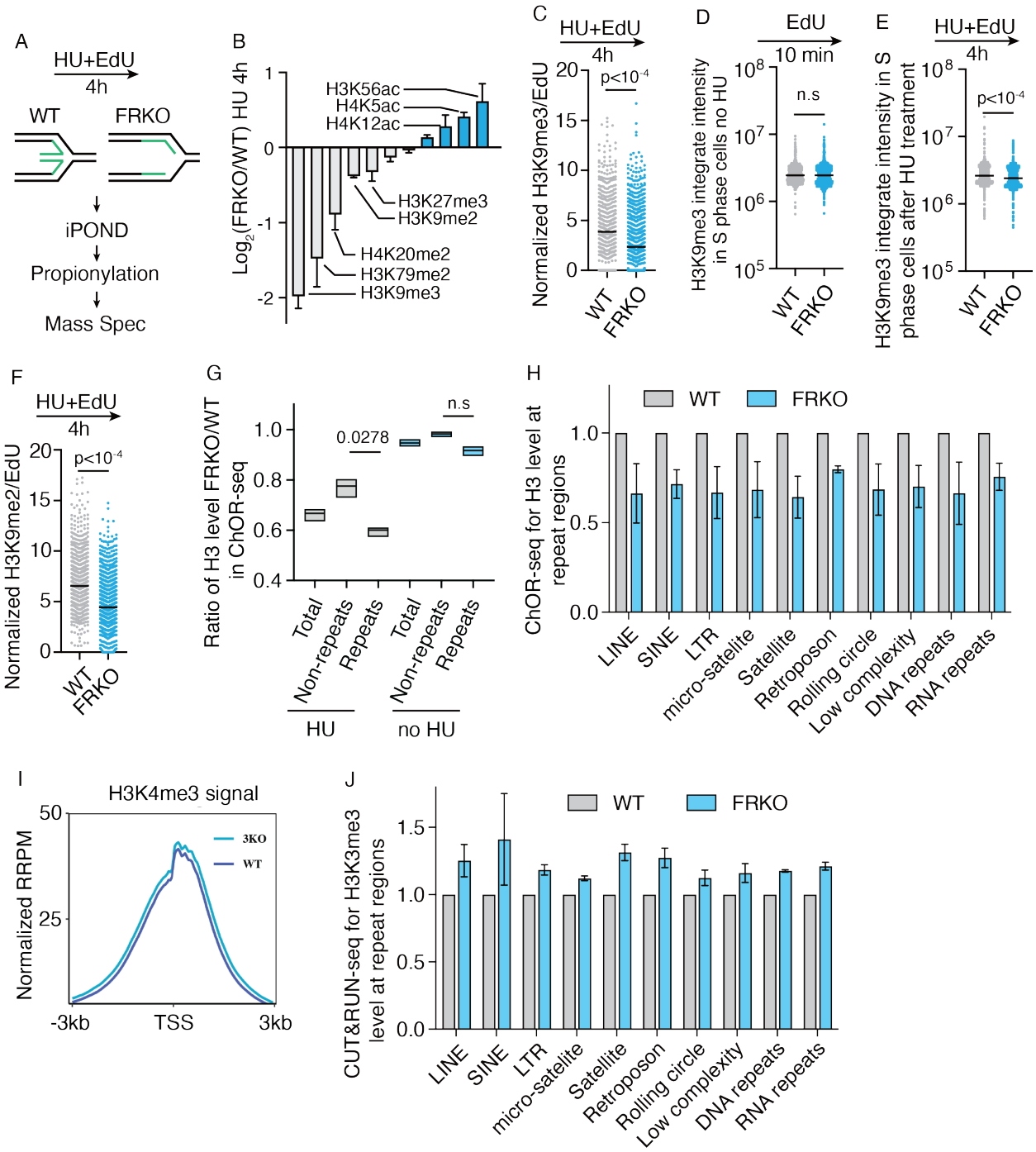

Figure 3 PrimPol deletion rescues low nucleosome density but compromise HU sensitivity

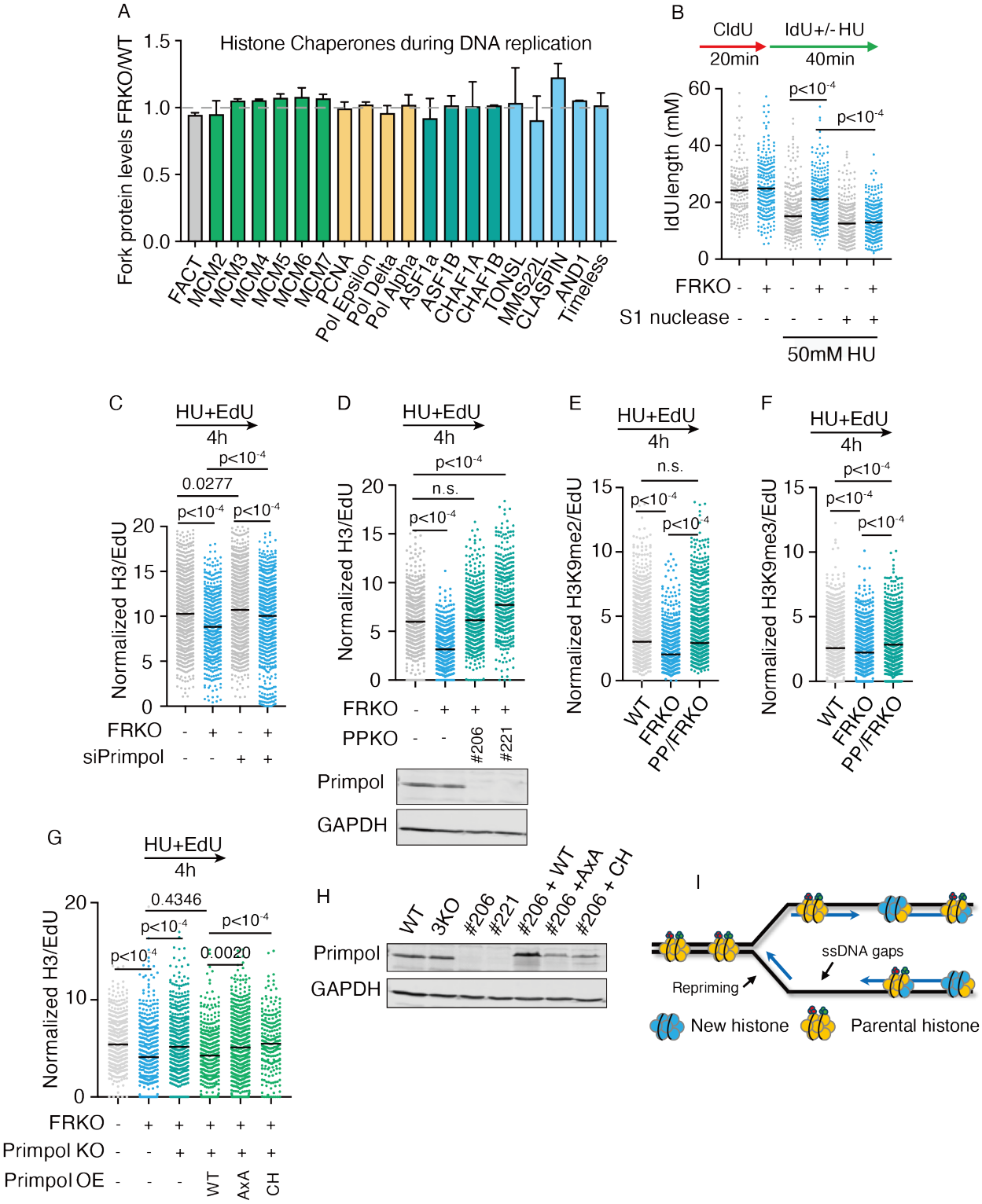

Figure 4 Single-Stranded DNA Gaps Decrease Nucleosome Density on Nascent DNA in Cells

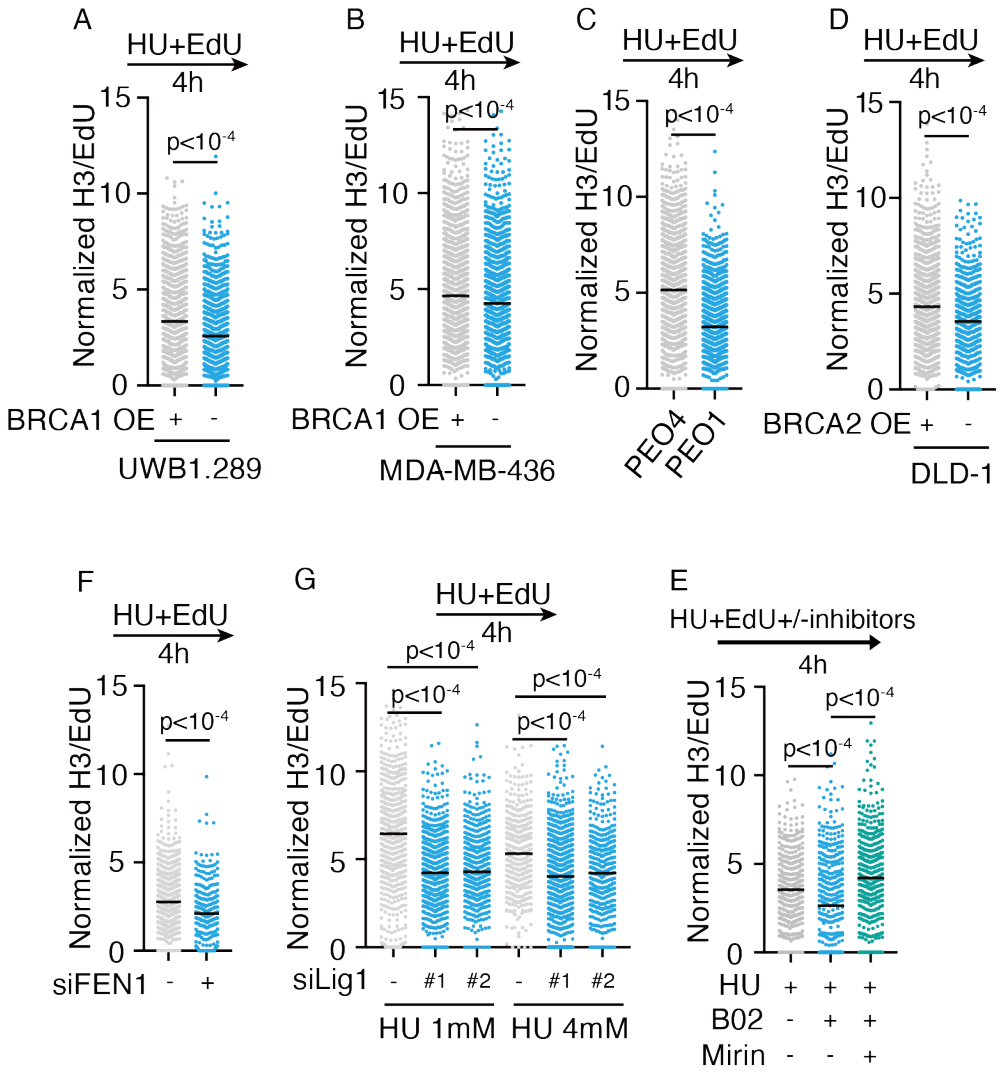

Figure 5 Nucleosomes can form on ssDNA gapped substrate in vitro

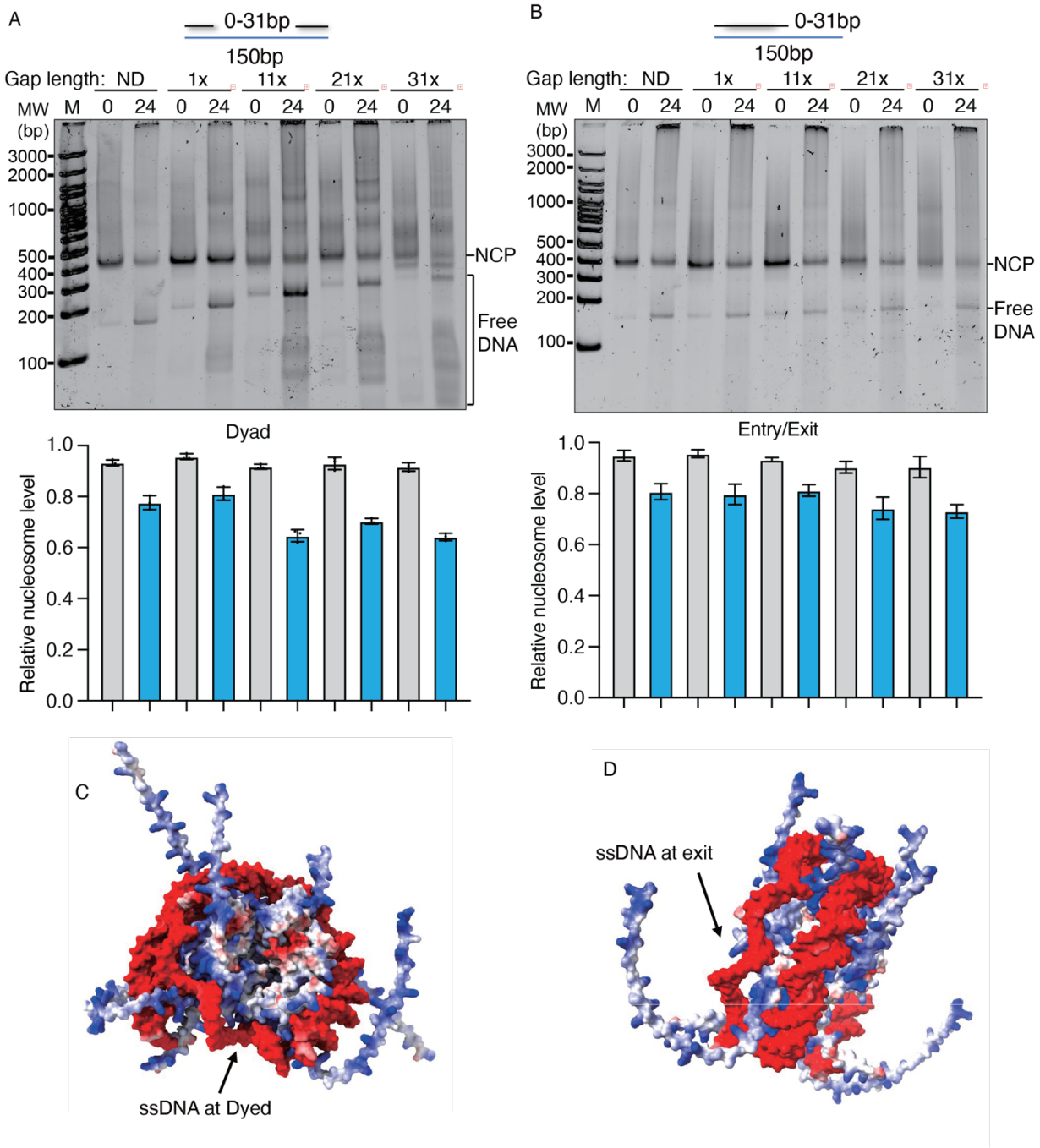

Figure 6 PARylation reduces nucleosome density in fork reversal deficient cells

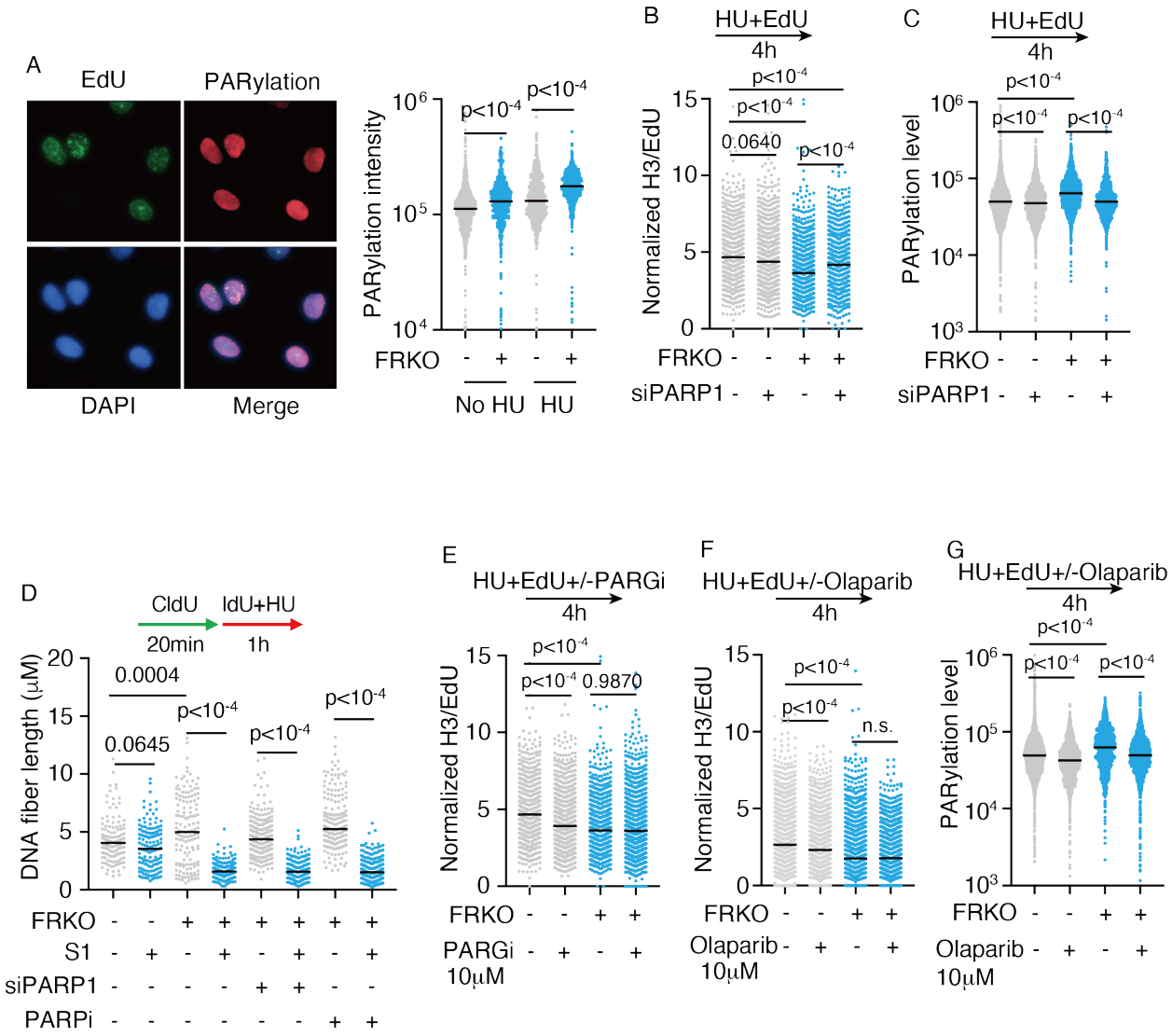

Figure 7 HMCES-DPC at ssDNA gaps reduces nucleosome density in fork reversal deficient cells

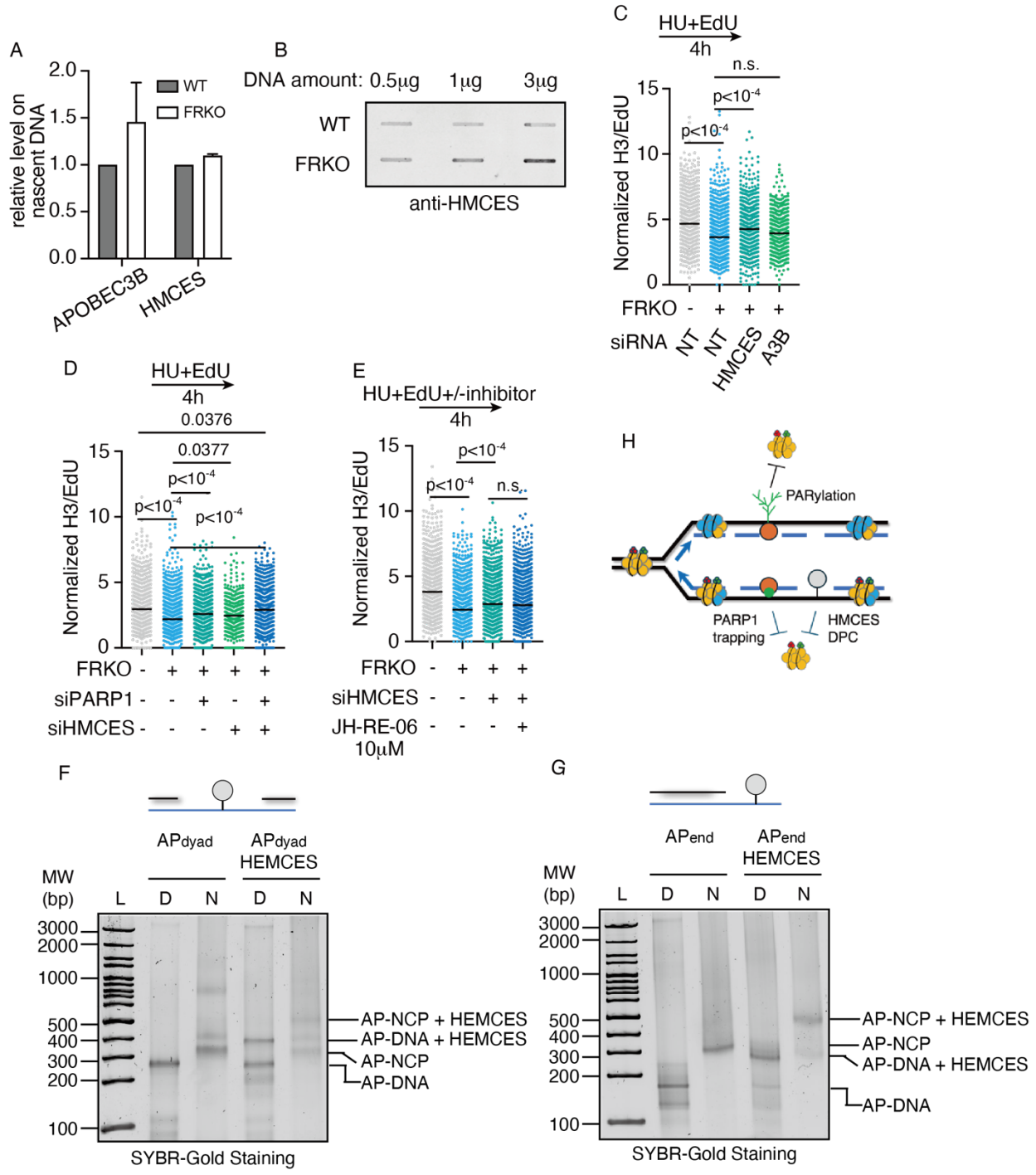

Figure S1 Fork reversal deficiency reduces the nucleosome density on nascent DNA

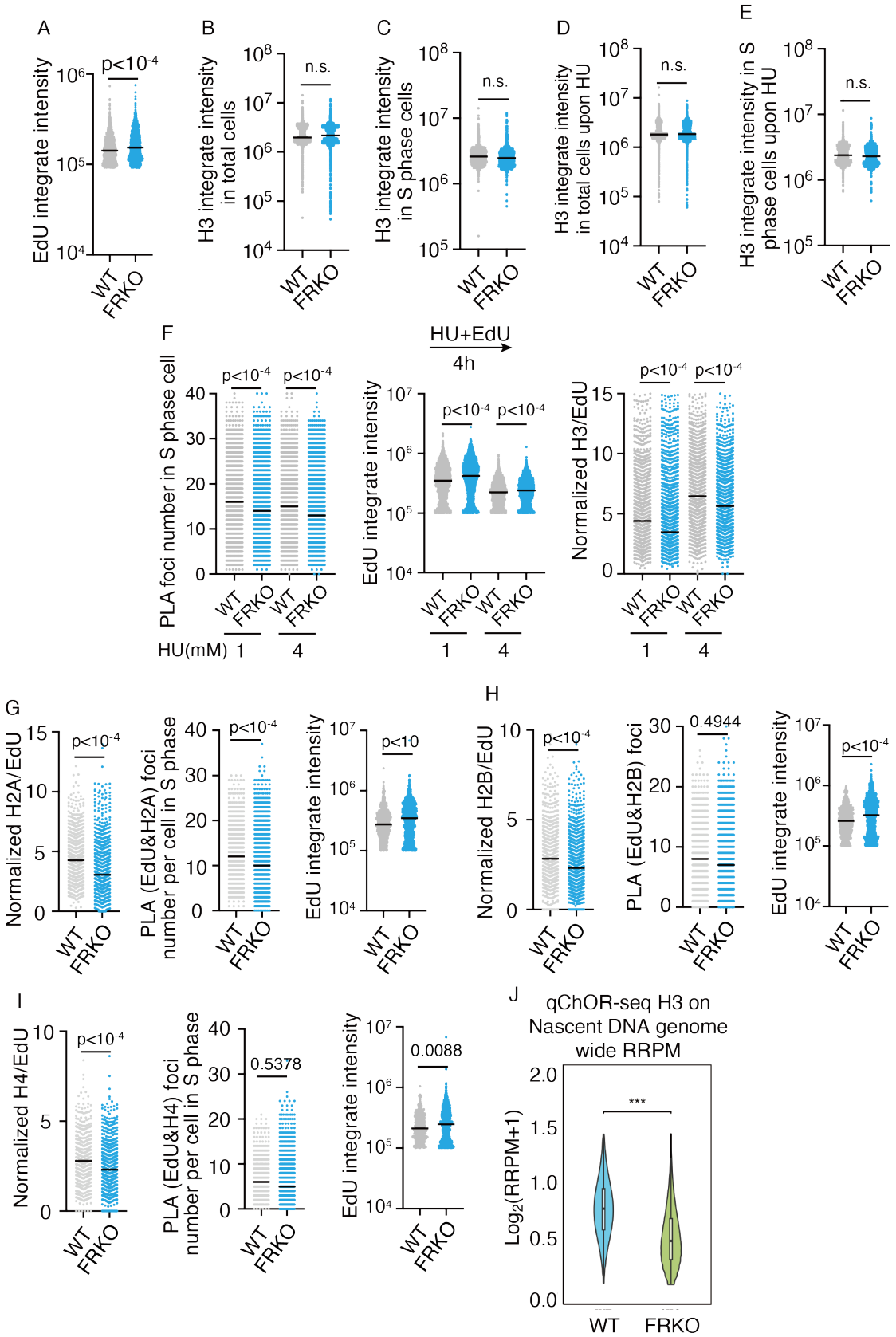

Figure S2 Low density of nucleosome is due to fork reversal deficiency rather than individual fork reversal enzyme depletion

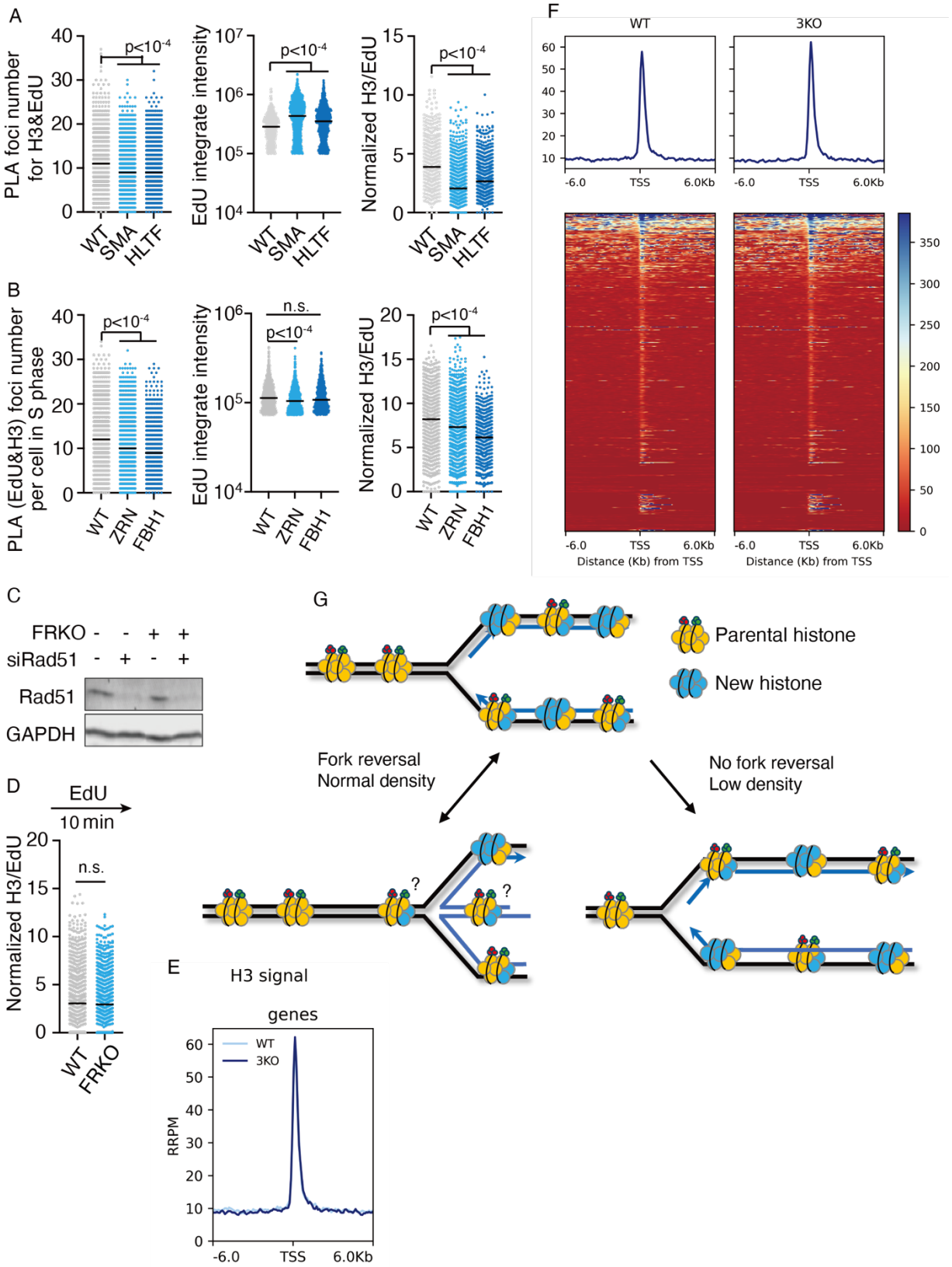

Figure S3 related to Figure 2 Fork reversal deficiency leads to parental histone loss

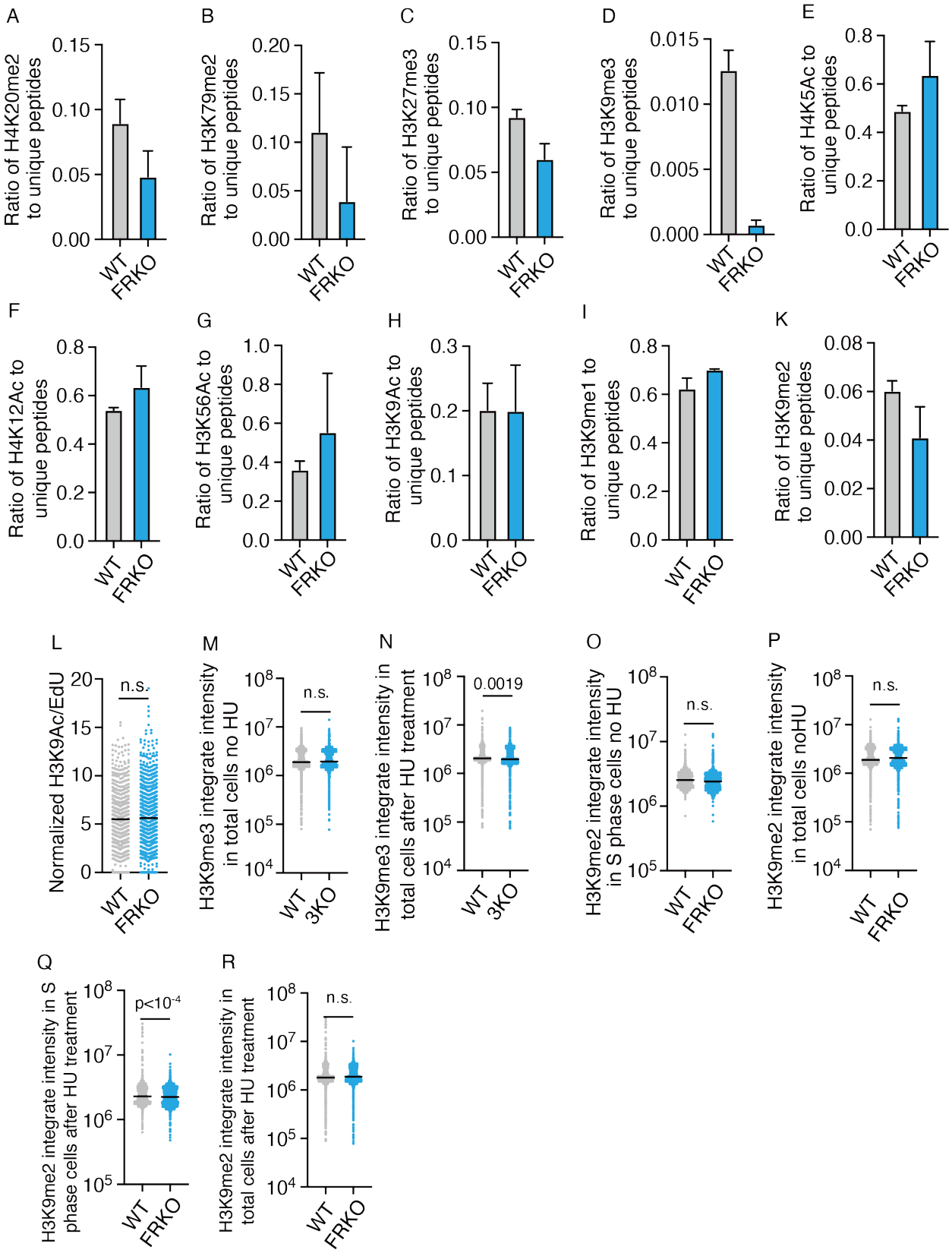

Figure S4 Fork reversal deficiency leads to primpol mediated ssDNA gaps and DNA damage

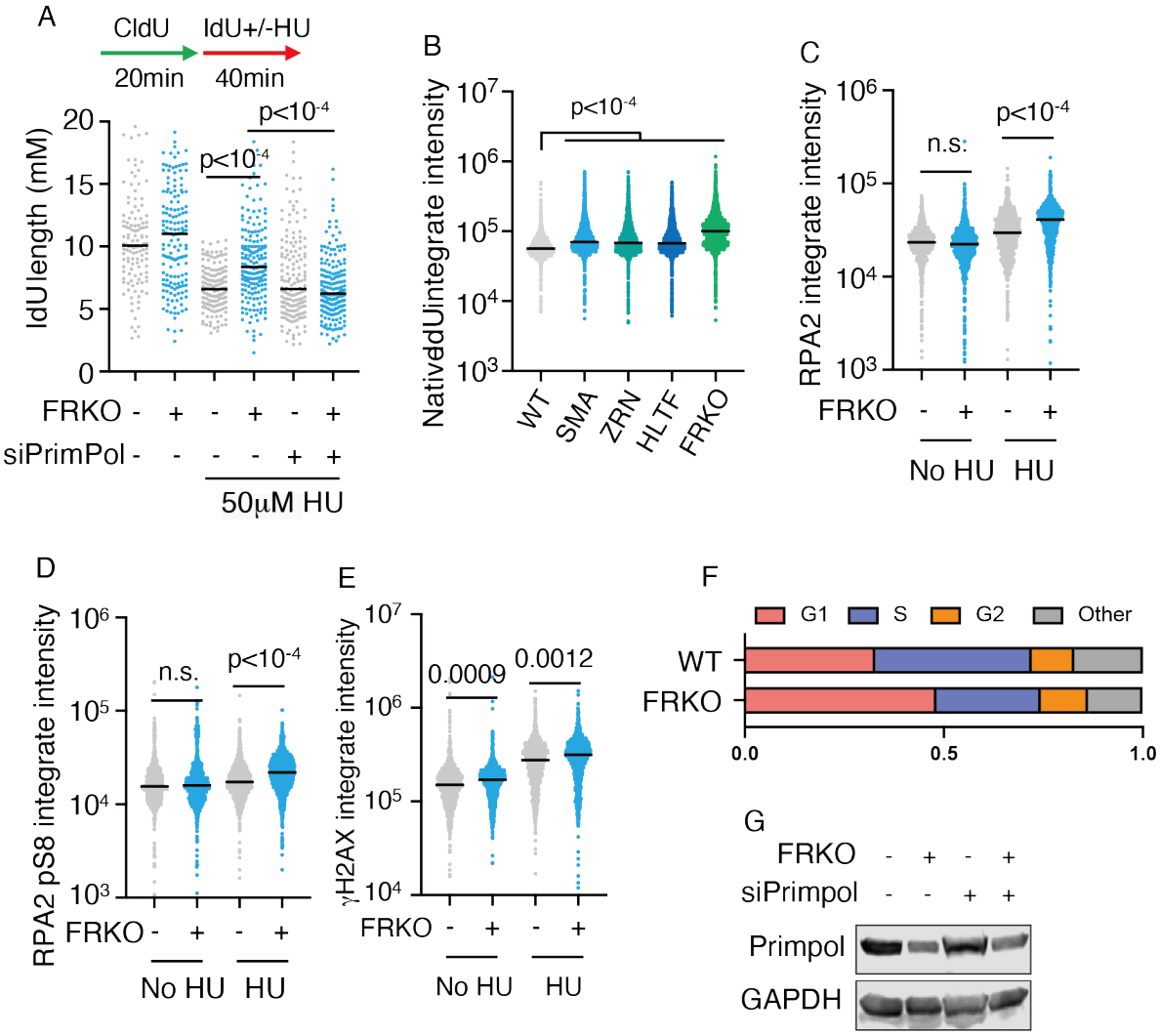

Figure S5 Single-stranded DNA gaps loosen the nucleosome assembly on nascent DNA in cells, related to Figure 4

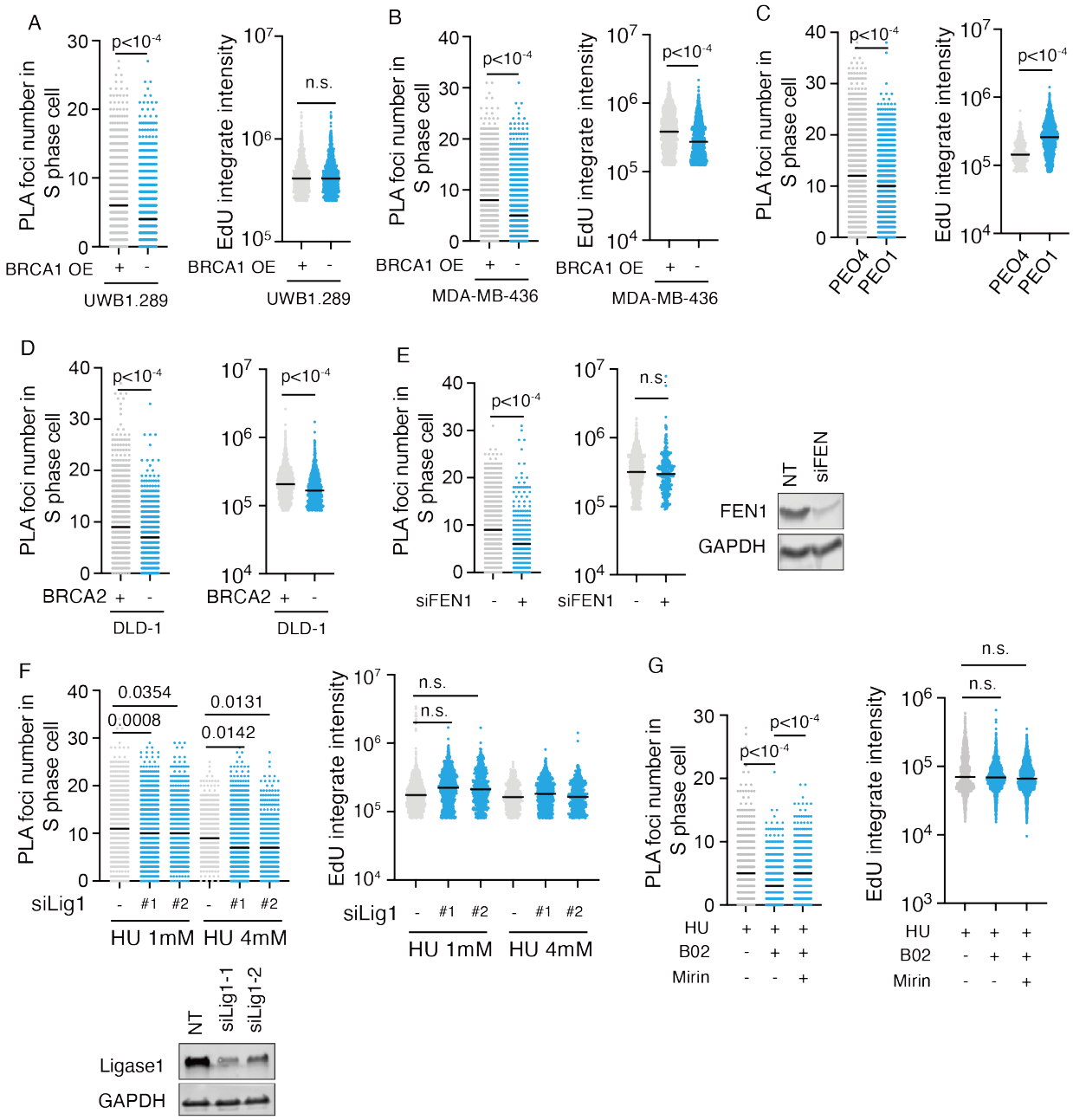

Figure S6 PARylation at ssDNA gaps reduces nucleosome density in fork reversal deficient cells

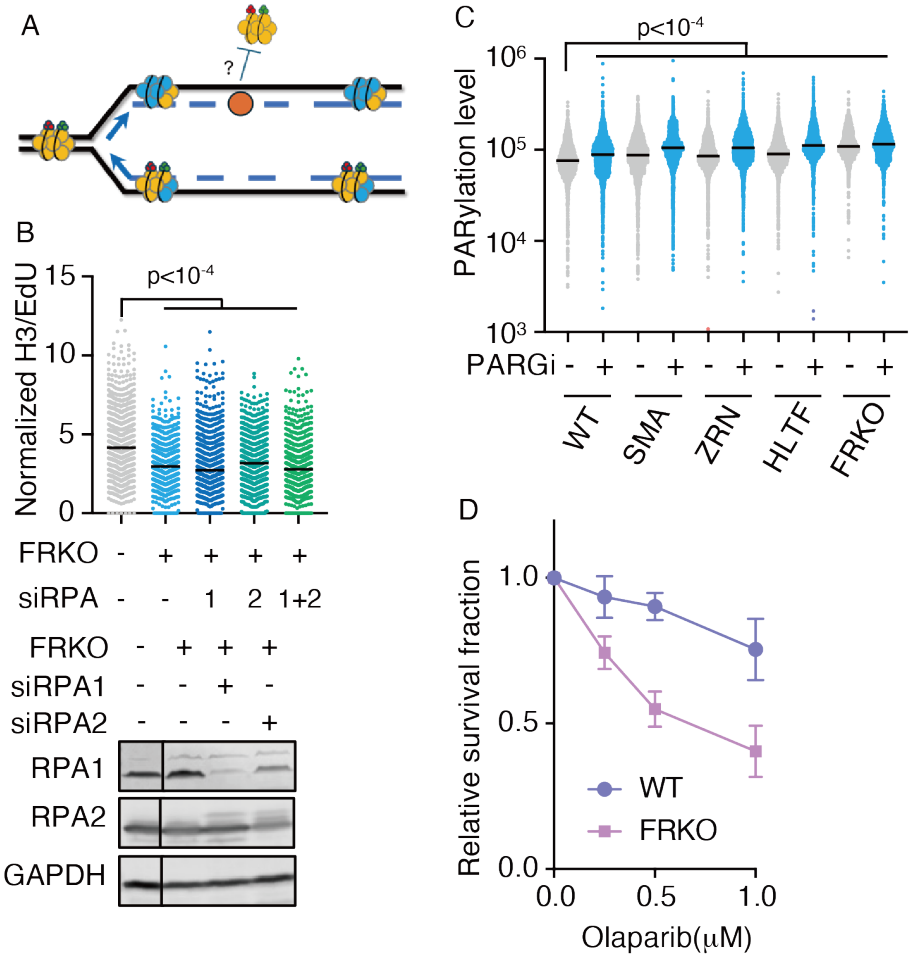

Figure S7 HMCES-DPC at ssDNA gaps reduces nucleosome density in fork reversal deficient cells

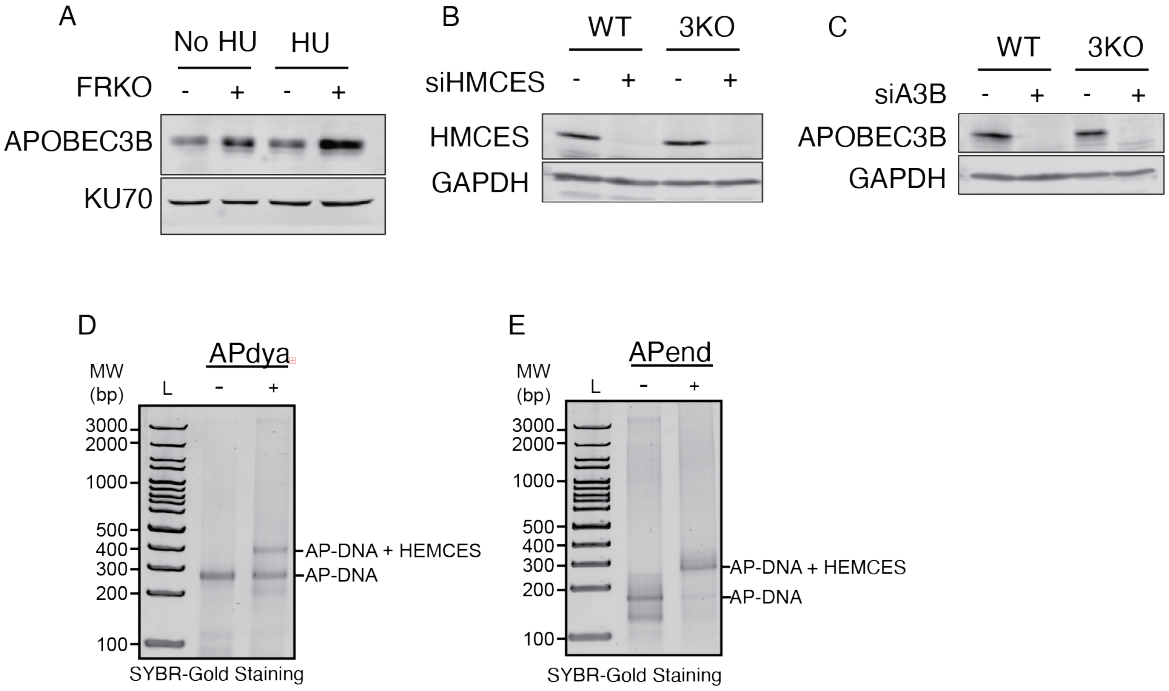

Reference

1. Stewart-Morgan, K.R., Petryk, N., and Groth, A. (2020). Chromatin replication and epigenetic cell memory. Nat Cell Biol *22*, 361-371. 10.1038/s41556-020-0487-y.
2. Alabert, C., and Groth, A. (2012). Chromatin replication and epigenome maintenance. Nature reviews Molecular cell biology *13*, 153-167.
3. Berti, M., Cortez, D., and Lopes, M. (2020). The plasticity of DNA replication forks in response to clinically relevant genotoxic stress. Nature reviews Molecular cell biology *21*, 633-651.
4. Allis, C.D., and Jenuwein, T. (2016). The molecular hallmarks of epigenetic control. Nature reviews genetics *17*, 487-500.
5. Cantone, I., and Fisher, A.G. (2013). Epigenetic programming and reprogramming during development. Nat Struct Mol Biol *20*, 282-289. 10.1038/nsmb.2489.
6. Suva, M.L., Riggi, N., and Bernstein, B.E. (2013). Epigenetic reprogramming in cancer. Science *339*, 1567-1570. 10.1126/science.1230184.
7. Iacobuzio-Donahue, C.A. (2009). Epigenetic changes in cancer. Annual Review of Pathology: Mechanisms of Disease *4*, 229-249.
8. Feinberg, A.P., Ohlsson, R., and Henikoff, S. (2006). The epigenetic progenitor origin of human cancer. Nature Reviews Genetics *7*, 21-33. 10.1038/nrg1748.
9. Feinberg, A.P., Koldobskiy, M.A., and Göndör, A. (2016). Epigenetic modulators, modifiers and mediators in cancer aetiology and progression. Nature Reviews Genetics *17*, 284-299. 10.1038/nrg.2016.13.

10. Easwaran, H., Tsai, H.-C., and Baylin, S.B. (2014). Cancer epigenetics: tumor heterogeneity, plasticity of stem-like states, and drug resistance. Molecular cell *54*, 716-727.

11. Li, N., Gao, Y., Zhang, Y., Yu, D., Lin, J., Feng, J., Li, J., Xu, Z., Zhang, Y., and Dang, S. (2024). Parental histone transfer caught at the replication fork. Nature *627*, 890-897.

12. Zhou, K., Gaullier, G., and Luger, K. (2019). Nucleosome structure and dynamics are coming of age. Nature structural & molecular biology *26*, 3-13.

13. Sekine, S.I., Ehara, H., Kujirai, T., and Kurumizaka, H. (2024). Structural perspectives on transcription in chromatin. Trends Cell Biol *34*, 211-224. 10.1016/j.tcb.2023.07.011.

14. Liu, Y., Zhou, K., Zhang, N., Wei, H., Tan, Y.Z., Zhang, Z., Carragher, B., Potter, C.S., D'Arcy, S., and Luger, K. (2020). FACT caught in the act of manipulating the nucleosome. Nature *577*, 426-431. 10.1038/s41586-019-1820-0.

15. Groth, A., Rocha, W., Verreault, A., and Almouzni, G. (2007). Chromatin challenges during DNA replication and repair. Cell *128*, 721-733. 10.1016/j.cell.2007.01.030.

16. Abe, T., Sugimura, K., Hosono, Y., Takami, Y., Akita, M., Yoshimura, A., Tada, S., Nakayama, T., Murofushi, H., and Okumura, K. (2011). The histone chaperone facilitates chromatin transcription (FACT) protein maintains normal replication fork rates. Journal of Biological Chemistry *286*, 30504-30512.

17. Tsunaka, Y., Fujiwara, Y., Oyama, T., Hirose, S., and Morikawa, K. (2016). Integrated molecular mechanism directing nucleosome reorganization by human FACT. Genes & development *30*, 673-686.

18. Wang, T., Liu, Y., Edwards, G., Krzizike, D., Scherman, H., and Luger, K. (2018). The histone chaperone FACT modulates nucleosome structure by tethering its components. Life science alliance *1*.

19. Wang, X., Tang, Y., Xu, J., Leng, H., Shi, G., Hu, Z., Wu, J., Xiu, Y., Feng, J., and Li, Q. (2023). The N-terminus of Spt16 anchors FACT to MCM2–7 for parental histone recycling. Nucleic acids research *51*, 11549-11567.

20. Escobar, T.M., Oksuz, O., Saldaña-Meyer, R., Descostes, N., Bonasio, R., and Reinberg, D. (2019). Active and repressed chromatin domains exhibit distinct nucleosome segregation during DNA replication. Cell *179*, 953-963. e911.

21. Madamba, E.V., Berthet, E.B., and Francis, N.J. (2017). Inheritance of histones H3 and H4 during DNA replication in vitro. Cell reports *21*, 1361-1374.

22. Schlissel, G., and Rine, J. (2019). The nucleosome core particle remembers its position through DNA replication and RNA transcription. Proceedings of the National Academy of Sciences *116*, 20605-20611.

23. Sauer, P.V., Gu, Y., Liu, W.H., Mattiroli, F., Panne, D., Luger, K., and Churchill, M.E. (2018). Mechanistic insights into histone deposition and nucleosome assembly by the chromatin assembly factor-1. Nucleic Acids Res *46*, 9907-9917. 10.1093/nar/gky823.

24. Stillman, B. (1986). Chromatin assembly during SV40 DNA replication in vitro. Cell *45*, 555-565.

25. Smith, S., and Stillman, B. (1989). Purification and characterization of CAF-I, a human cell factor required for chromatin assembly during DNA replication in vitro. Cell *58*, 15-25.

26. Shibahara, K.-i., and Stillman, B. (1999). Replication-dependent marking of DNA by PCNA facilitates CAF-1-coupled inheritance of chromatin. Cell *96*, 575-585.

27. Groth, A., Corpet, A., Cook, A.J., Roche, D., Bartek, J., Lukas, J., and Almouzni, G. (2007). Regulation of replication fork progression through histone supply and demand. science *318*, 1928-1931.

28. Richet, N., Liu, D., Legrand, P., Velours, C., Corpet, A., Gaubert, A., Bakail, M., Moal-Raisin, G., Guerois, R., and Compper, C. (2015). Structural insight into how the human helicase subunit MCM2 may act as a histone chaperone together with ASF1 at the replication fork. Nucleic acids research *43*, 1905-1917.

29. Wang, H., Wang, M., Yang, N., and Xu, R.-M. (2015). Structure of the quaternary complex of histone H3-H4 heterodimer with chaperone ASF1 and the replicative helicase subunit MCM2. Protein & cell *6*, 693-697.

30. Alabert, C., Barth, T.K., Reverón-Gómez, N., Sidoli, S., Schmidt, A., Jensen, O.N., Imhof, A., and Groth, A. (2015). Two distinct modes for propagation of histone PTMs across the cell cycle. Genes & development *29*, 585-590.

31. Reverón-Gómez, N., González-Aguilera, C., Stewart-Morgan, K.R., Petryk, N., Flury, V., Graziano, S., Johansen, J.V., Jakobsen, J.S., Alabert, C., and Groth, A. (2018). Accurate recycling of parental histones reproduces the histone modification landscape during DNA replication. Molecular cell *72*, 239-249. e235.

32. Reinberg, D., and Vales, L.D. (2018). Chromatin domains rich in inheritance. Science *361*, 33-34.

33. Oksuz, O., Narendra, V., Lee, C.-H., Descostes, N., LeRoy, G., Raviram, R., Blumenberg, L., Karch, K., Rocha, P.P., and Garcia, B.A. (2018). Capturing the onset of PRC2-mediated repressive domain formation. Molecular cell *70*, 1149-1162. e1145.

34. Alabert, C., Loos, C., Voelker-Albert, M., Graziano, S., Forné, I., Reveron-Gomez, N., Schuh, L., Hasenauer, J., Marr, C., and Imhof, A. (2020). Domain model explains propagation dynamics and stability of histone H3K27 and H3K36 methylation landscapes. Cell reports *30*, 1223-1234. e1228.

35. López, V.G., Valencia-Sánchez, M.I., Abini-Agbomson, S., Thomas, J.F., Lee, R., De Ioannes, P., Sosa, B.A., Armache, J.-P., and Armache, K.-J. (2024). Read–write mechanisms of H2A ubiquitination by Polycomb repressive complex 1. Nature *636*, 755-761.

36. Hathaway, N.A., Bell, O., Hodges, C., Miller, E.L., Neel, D.S., and Crabtree, G.R. (2012). Dynamics and memory of heterochromatin in living cells. Cell *149*, 1447-1460.

37. Gan, H., Serra-Cardona, A., Hua, X., Zhou, H., Labib, K., Yu, C., and Zhang, Z. (2018). The Mcm2-Ctf4-Polalpha Axis Facilitates Parental Histone H3-H4 Transfer to Lagging Strands. Mol Cell *72*, 140-151 e143. 10.1016/j.molcel.2018.09.001.

38. Petryk, N., Dalby, M., Wenger, A., Stromme, C.B., Strandsby, A., Andersson, R., and Groth, A. (2018). MCM2 promotes symmetric inheritance of modified histones during DNA replication. Science *361*, 1389-1392. 10.1126/science.aau0294.

39. Huang, H., Strømme, C.B., Saredi, G., Hödl, M., Strandsby, A., González-Aguilera, C., Chen, S., Groth, A., and Patel, D.J. (2015). A unique binding mode enables MCM2 to chaperone histones H3–H4 at replication forks. Nature structural & molecular biology *22*, 618-626.

40. Tian, C., Zhang, Q., Jia, J., Zhou, J., Zhang, Z., Karri, S., Jiang, J., Dickinson, Q., Yao, Y., Tang, X., et al. (2024). DNA polymerase delta governs parental histone transfer to DNA replication lagging strand. Proc Natl Acad Sci U S A *121*, e2400610121. 10.1073/pnas.2400610121.

41. Serra-Cardona, A., Hua, X., McNutt, S.W., Zhou, H., Toda, T., Jia, S., Chu, F., and Zhang, Z. (2024). The PCNA-Pol delta complex couples lagging strand DNA synthesis to parental histone transfer for epigenetic inheritance. Sci Adv *10*, eadn5175. 10.1126/sciadv.adn5175.

42. Charlton, S.J., Flury, V., Kanoh, Y., Genzor, A.V., Kollenstart, L., Ao, W., Brogger, P., Weisser, M.B., Adamus, M., Alcaraz, N., et al. (2024). The fork protection complex promotes parental histone recycling and epigenetic memory. Cell *187*, 5029-5047 e5021. 10.1016/j.cell.2024.07.017.

43. Gambus, A., Van Deursen, F., Polychronopoulos, D., Foltman, M., Jones, R.C., Edmondson, R.D., Calzada, A., and Labib, K. (2009). A key role for Ctf4 in coupling the MCM2-7 helicase to DNA polymerase α within the eukaryotic replisome. The EMBO journal *28*, 2992-3004.

44. Simon, A.C., Zhou, J.C., Perera, R.L., van Deursen, F., Evrin, C., Ivanova, M.E., Kilkenny, M.L., Renault, L., Kjaer, S., and Matak-Vinković, D. (2014). A Ctf4 trimer couples the CMG helicase to DNA polymerase α in the eukaryotic replisome. Nature *510*, 293-297.

45. Evrin, C., Maman, J.D., Diamante, A., Pellegrini, L., and Labib, K. (2018). Histone H2A-H2B binding by Pol α in the eukaryotic replisome contributes to the maintenance of repressive chromatin. The EMBO journal *37*, e99021.

46. Katou, Y., Kanoh, Y., Bando, M., Noguchi, H., Tanaka, H., Ashikari, T., Sugimoto, K., and Shirahige, K. (2003). S-phase checkpoint proteins Tof1 and Mrc1 form a stable replication-pausing complex. Nature *424*, 1078-1083.

47. Toda, T., Fang, Y., Shan, C.-M., Hua, X., Kim, J.-K., Tang, L.C., Jovanovic, M., Tong, L., Qiao, F., and Zhang, Z. (2024). Mrc1 regulates parental histone segregation and heterochromatin inheritance. Molecular Cell *84*, 3223-3236. e3224.

48. Li, Z., Duan, S., Hua, X., Xu, X., Li, Y., Menolfi, D., Zhou, H., Lu, C., Zha, S., Goff, S.P., and Zhang, Z. (2023). Asymmetric distribution of parental H3K9me3 in S phase silences L1 elements. Nature *623*, 643-651. 10.1038/s41586-023-06711-3.

49. Kollenstart, L., Biran, A., Alcaraz, N., Reverón-Gómez, N., Solis-Mezarino, V., Völker-Albert, M., Jenkinson, F., Flury, V., and Groth, A. (2025). Disabling leading and lagging strand histone transmission results in parental histones loss and reduced cell plasticity and viability. Science Advances *11*, eadr1453. doi:10.1126/sciadv.adr1453.

50. Saxena, S., and Zou, L. (2022). Hallmarks of DNA replication stress. Mol Cell *82*, 2298-2314. 10.1016/j.molcel.2022.05.004.

51. Zellweger, R., Dalcher, D., Mutreja, K., Berti, M., Schmid, J.A., Herrador, R., Vindigni, A., and Lopes, M. (2015). Rad51-mediated replication fork reversal is a global response to genotoxic treatments in human cells. J Cell Biol *208*, 563-579. 10.1083/jcb.201406099.

52. Liu, W., Saito, Y., Jackson, J., Bhowmick, R., Kanemaki, M.T., Vindigni, A., and Cortez, D. (2023). RAD51 bypasses the CMG helicase to promote replication fork reversal. Science *380*, 382-387. doi:10.1126/science.add7328.

53. Poole, L.A., and Cortez, D. (2017). Functions of SMARCAL1, ZRANB3, and HLTF in maintaining genome stability. Critical reviews in biochemistry and molecular biology *52*, 696-714.

54. Adolph, M.B., Warren, G.M., Couch, F.B., Greer, B.H., Eichman, B.F., and Cortez, D. (2024). Strand dependent bypass of DNA lesions during fork reversal by ATP-dependent translocases SMARCAL1, ZRANB3, and HLTF. bioRxiv, 2024.2009. 2017.613558.

55. Couch, F.B., Bansbach, C.E., Driscoll, R., Luzwick, J.W., Glick, G.G., Bétous, R., Carroll, C.M., Jung, S.Y., Qin, J., and Cimprich, K.A. (2013). ATR phosphorylates SMARCAL1 to prevent replication fork collapse. Genes & development *27*, 1610-1623.

56. Bétous, R., Mason, A.C., Rambo, R.P., Bansbach, C.E., Badu-Nkansah, A., Sirbu, B.M., Eichman, B.F., and Cortez, D. (2012). SMARCAL1 catalyzes fork regression and Holliday junction migration to maintain genome stability during DNA replication. Genes & development *26*, 151-162.

57. Ciccia, A., Nimonkar, A.V., Hu, Y., Hajdu, I., Achar, Y.J., Izhar, L., Petit, S.A., Adamson, B., Yoon, J.C., and Kowalczykowski, S.C. (2012). Polyubiquitinated PCNA recruits the ZRANB3 translocase to maintain genomic integrity after replication stress. Molecular cell *47*, 396-409.

58. Vujanovic, M., Krietsch, J., Raso, M.C., Terraneo, N., Zellweger, R., Schmid, J.A., Taglialatela, A., Huang, J.-W., Holland, C.L., and Zwicky, K. (2017). Replication fork slowing and reversal upon DNA damage require PCNA polyubiquitination and ZRANB3 DNA translocase activity. Molecular cell *67*, 882-890. e885.

59. Kile, A.C., Chavez, D.A., Bacal, J., Eldirany, S., Korzhnev, D.M., Bezsonova, I., Eichman, B.F., and Cimprich, K.A. (2015). HLTF's ancient HIRAN domain binds 3′ DNA ends to drive replication fork reversal. Molecular cell *58*, 1090-1100.

60. Achar, Y.J., Balogh, D., and Haracska, L. (2011). Coordinated protein and DNA remodeling by human HLTF on stalled replication fork. Proceedings of the National Academy of Sciences *108*, 14073-14078.

61. Blastyák, A., Pintér, L., Unk, I., Prakash, L., Prakash, S., and Haracska, L. (2007). Yeast Rad5 protein required for postreplication repair has a DNA helicase activity specific for replication fork regression. Molecular cell *28*, 167-175.

62. Blastyák, A., Hajdú, I., Unk, I., and Haracska, L. (2010). Role of double-stranded DNA translocase activity of human HLTF in replication of damaged DNA. Molecular and cellular biology *30*, 684-693.

63. Bai, G., Kermi, C., Stoy, H., Schiltz, C.J., Bacal, J., Zaino, A.M., Hadden, M.K., Eichman, B.F., Lopes, M., and Cimprich, K.A. (2020). HLTF promotes fork reversal, limiting

replication stress resistance and preventing multiple mechanisms of unrestrained DNA synthesis. Molecular cell *78*, 1237-1251. e1237.

64. Quinet, A., Tirman, S., Jackson, J., Šviković, S., Lemaçon, D., Carvajal-Maldonado, D., González-Acosta, D., Vessoni, A.T., Cybulla, E., and Wood, M. (2020). PRIMPOL-mediated adaptive response suppresses replication fork reversal in BRCA-deficient cells. Molecular cell *77*, 461-474. e469.

65. Taglialatela, A., Leuzzi, G., Sannino, V., Cuella-Martin, R., Huang, J.W., Wu-Baer, F., Baer, R., Costanzo, V., and Ciccia, A. (2021). REV1-Polζ maintains the viability of homologous recombination-deficient cancer cells through mutagenic repair of PRIMPOL-dependent ssDNA gaps. Mol Cell *81*, 4008-4025.e4007. 10.1016/j.molcel.2021.08.016.

66. Cong, K., Peng, M., Kousholt, A.N., Lee, W.T.C., Lee, S., Nayak, S., Krais, J., VanderVere-Carozza, P.S., Pawelczak, K.S., Calvo, J., et al. (2021). Replication gaps are a key determinant of PARP inhibitor synthetic lethality with BRCA deficiency. Mol Cell *81*, 3128-3144.e3127. 10.1016/j.molcel.2021.06.011.

67. Cong, K., and Cantor, S.B. (2022). Exploiting replication gaps for cancer therapy. Mol Cell *82*, 2363-2369. 10.1016/j.molcel.2022.04.023.

68. Li, Z., Hua, X., Serra-Cardona, A., Xu, X., Gan, S., Zhou, H., Yang, W.-S., Chen, C.-l., Xu, R.-M., and Zhang, Z. (2020). DNA polymerase α interacts with H3-H4 and facilitates the transfer of parental histones to lagging strands. Science advances *6*, eabb5820.

69. Treangen, T.J., and Salzberg, S.L. (2012). Repetitive DNA and next-generation sequencing: computational challenges and solutions. Nature Reviews Genetics *13*, 36-46. 10.1038/nrg3117.

70. Petryk, N., Reveron-Gomez, N., Gonzalez-Aguilera, C., Dalby, M., Andersson, R., and Groth, A. (2021). Genome-wide and sister chromatid-resolved profiling of protein occupancy in replicated chromatin with ChOR-seq and SCAR-seq. Nature Protocols *16*, 4446-4493.

71. Sun, Z., Filipescu, D., Andrade, J., Gaspar-Maia, A., Ueberheide, B., and Bernstein, E. (2018). Transcription-associated histone pruning demarcates macroH2A chromatin domains. Nature Structural & Molecular Biology *25*, 958-970. 10.1038/s41594-018-0134-5.

72. Tagami, H., Ray-Gallet, D., Almouzni, G., and Nakatani, Y. (2004). Histone H3. 1 and H3. 3 complexes mediate nucleosome assembly pathways dependent or independent of DNA synthesis. Cell *116*, 51-61.

73. Jansen , L.E.T., Black , B.E., Foltz , D.R., and Cleveland , D.W. (2007). Propagation of centromeric chromatin requires exit from mitosis. Journal of Cell Biology *176*, 795-805. 10.1083/jcb.200701066.

74. Rouillon, C., Eckhardt, B.V., Kollenstart, L., Gruss, F., Verkennis, Alexander E.E., Rondeel, I., Krijger, P.H.L., Ricci, G., Biran, A., van Laar, T., et al. (2023). CAF-1 deposits newly synthesized histones during DNA replication using distinct mechanisms on the leading and lagging strands. Nucleic Acids Research *51*, 3770-3792. 10.1093/nar/gkad171.

75. Wenger, A., Biran, A., Alcaraz, N., Redó-Riveiro, A., Sell, A.C., Krautz, R., Flury, V., Reverón-Gómez, N., Solis-Mezarino, V., Völker-Albert, M., et al. (2023). Symmetric inheritance of parental histones governs epigenome maintenance and embryonic stem cell identity. Nature Genetics *55*, 1567-1578. 10.1038/s41588-023-01476-x.

76. Tirman, S., Quinet, A., Wood, M., Meroni, A., Cybulla, E., Jackson, J., Pegoraro, S., Simoneau, A., Zou, L., and Vindigni, A. (2021). Temporally distinct post-replicative repair mechanisms fill PRIMPOL-dependent ssDNA gaps in human cells. Mol Cell *81*, 4026-4040.e4028. 10.1016/j.molcel.2021.09.013.

77. Schlacher, K., Wu, H., and Jasin, M. (2012). A Distinct Replication Fork Protection Pathway Connects Fanconi Anemia Tumor Suppressors to RAD51-BRCA1/2. Cancer Cell *22*, 106-116. https://doi.org/10.1016/j.ccr.2012.05.015.

78. Schlacher, K., Christ, N., Siaud, N., Egashira, A., Wu, H., and Jasin, M. (2011). Double-Strand Break Repair-Independent Role for BRCA2 in Blocking Stalled Replication Fork Degradation by MRE11. Cell *145*, 529-542. https://doi.org/10.1016/j.cell.2011.03.041.

79. Kang, Z., Fu, P., Alcivar, A.L., Fu, H., Redon, C., Foo, T.K., Zuo, Y., Ye, C., Baxley, R., Madireddy, A., et al. (2021). BRCA2 associates with MCM10 to suppress PRIMPOL-mediated repriming and single-stranded gap formation after DNA damage. Nature Communications *12*, 5966. 10.1038/s41467-021-26227-6.

80. Taglialatela, A., Alvarez, S., Leuzzi, G., Sannino, V., Ranjha, L., Huang, J.-W., Madubata, C., Anand, R., Levy, B., Rabadan, R., et al. (2017). Restoration of Replication Fork Stability in BRCA1- and BRCA2-Deficient Cells by Inactivation of SNF2-Family Fork

Remodelers. Molecular Cell *68*, 414-430.e418. https://doi.org/10.1016/j.molcel.2017.09.036.

81. Thakar, T., Dhoonmoon, A., Straka, J., Schleicher, E.M., Nicolae, C.M., and Moldovan, G.-L. (2022). Lagging strand gap suppression connects BRCA-mediated fork protection to nucleosome assembly through PCNA-dependent CAF-1 recycling. Nature Communications *13*, 5323. 10.1038/s41467-022-33028-y.

82. Hashimoto, Y., Ray Chaudhuri, A., Lopes, M., and Costanzo, V. (2010). Rad51 protects nascent DNA from Mre11-dependent degradation and promotes continuous DNA synthesis. Nature Structural & Molecular Biology *17*, 1305-1311. 10.1038/nsmb.1927.

83. Bantele, S.C.S., Lisby, M., and Pfander, B. (2019). Quantitative sensing and signalling of single-stranded DNA during the DNA damage response. Nat Commun *10*, 944. 10.1038/s41467-019-08889-5.

84. Chen, C.C., Carson, J.J., Feser, J., Tamburini, B., Zabaronick, S., Linger, J., and Tyler, J.K. (2008). Acetylated lysine 56 on histone H3 drives chromatin assembly after repair and signals for the completion of repair. Cell *134*, 231-243. 10.1016/j.cell.2008.06.035.

85. Mimitou, E.P., Yamada, S., and Keeney, S. (2017). A global view of meiotic double-strand break end resection. Science *355*, 40-45. 10.1126/science.aak9704.

86. Tsukuda, T., Fleming, A.B., Nickoloff, J.A., and Osley, M.A. (2005). Chromatin remodelling at a DNA double-strand break site in Saccharomyces cerevisiae. Nature *438*, 379-383. 10.1038/nature04148.

87. Tsukuda, T., Lo, Y.C., Krishna, S., Sterk, R., Osley, M.A., and Nickoloff, J.A. (2009). INO80-dependent chromatin remodeling regulates early and late stages of mitotic homologous recombination. DNA Repair (Amst) *8*, 360-369. 10.1016/j.dnarep.2008.11.014.

88. van Attikum, H., Fritsch, O., and Gasser, S.M. (2007). Distinct roles for SWR1 and INO80 chromatin remodeling complexes at chromosomal double-strand breaks. Embo j *26*, 4113-4125. 10.1038/sj.emboj.7601835.

89. Peritore, M., Reusswig, K.U., Bantele, S.C.S., Straub, T., and Pfander, B. (2021). Strand-specific ChIP-seq at DNA breaks distinguishes ssDNA versus dsDNA binding and refutes single-stranded nucleosomes. Mol Cell *81*, 1841-1853.e1844. 10.1016/j.molcel.2021.02.005.

90. Palter, K.B., Foe, V.E., and Alberts, B.M. (1979). Evidence for the formation of nucleosome-like histone complexes on single-stranded DNA. Cell *18*, 451-467. 10.1016/0092-8674(79)90064-3.

91. Adkins, N.L., Swygert, S.G., Kaur, P., Niu, H., Grigoryev, S.A., Sung, P., Wang, H., and Peterson, C.L. (2017). Nucleosome-like, Single-stranded DNA (ssDNA)-Histone Octamer Complexes and the Implication for DNA Double Strand Break Repair. J Biol Chem *292*, 5271-5281. 10.1074/jbc.M117.776369.

92. Huang, T.H., Fowler, F., Chen, C.C., Shen, Z.J., Sleckman, B., and Tyler, J.K. (2018). The Histone Chaperones ASF1 and CAF-1 Promote MMS22L-TONSL-Mediated Rad51 Loading onto ssDNA during Homologous Recombination in Human Cells. Mol Cell *69*, 879-892.e875. 10.1016/j.molcel.2018.01.031.

93. Ray Chaudhuri, A., and Nussenzweig, A. (2017). The multifaceted roles of PARP1 in DNA repair and chromatin remodelling. Nat Rev Mol Cell Biol *18*, 610-621. 10.1038/nrm.2017.53.

94. Bacic, L., Gaullier, G., Sabantsev, A., Lehmann, L.C., Brackmann, K., Dimakou, D., Halic, M., Hewitt, G., Boulton, S.J., and Deindl, S. (2021). Structure and dynamics of the chromatin remodeler ALC1 bound to a PARylated nucleosome. Elife *10*. 10.7554/eLife.71420.

95. Lehmann, L.C., Hewitt, G., Aibara, S., Leitner, A., Marklund, E., Maslen, S.L., Maturi, V., Chen, Y., van der Spoel, D., Skehel, J.M., et al. (2017). Mechanistic Insights into Autoinhibition of the Oncogenic Chromatin Remodeler ALC1. Mol Cell *68*, 847-859.e847. 10.1016/j.molcel.2017.10.017.

96. Yang, G., Chen, Y., Wu, J., Chen, S.H., Liu, X., Singh, A.K., and Yu, X. (2020). Poly(ADP-ribosyl)ation mediates early phase histone eviction at DNA lesions. Nucleic Acids Res *48*, 3001-3013. 10.1093/nar/gkaa022.

97. Nosella, M.L., Kim, T.H., Huang, S.K., Harkness, R.W., Goncalves, M., Pan, A., Tereshchenko, M., Vahidi, S., Rubinstein, J.L., Lee, H.O., et al. (2024). Poly(ADP-ribosyl)ation enhances nucleosome dynamics and organizes DNA damage repair components within biomolecular condensates. Mol Cell *84*, 429-446.e417. 10.1016/j.molcel.2023.12.019.

98. Poirier, G.G., de Murcia, G., Jongstra-Bilen, J., Niedergang, C., and Mandel, P. (1982). Poly(ADP-ribosyl)ation of polynucleosomes causes relaxation of chromatin structure. Proc Natl Acad Sci U S A *79*, 3423-3427. 10.1073/pnas.79.11.3423.

99. Strickfaden, H., McDonald, D., Kruhlak, M.J., Haince, J.F., Th'ng, J.P.H., Rouleau, M., Ishibashi, T., Corry, G.N., Ausio, J., Underhill, D.A., et al. (2016). Poly(ADP-ribosyl)ation-dependent Transient Chromatin Decondensation and Histone Displacement following Laser Microirradiation. J Biol Chem *291*, 1789-1802. 10.1074/jbc.M115.694992.

100. Moser, S.C., Khalizieva, A., Roehsner, J., Pottendorfer, E., Kaptein, M.L., Ricci, G., Bhardwaj, V., Bleijerveld, O.B., Hoekman, L., van der Heijden, I., et al. (2025). NASP modulates histone turnover to drive PARP inhibitor resistance. Nature. 10.1038/s41586-025-09414-z.

101. Pecori, R., Di Giorgio, S., Paulo Lorenzo, J., and Nina Papavasiliou, F. (2022). Functions and consequences of AID/APOBEC-mediated DNA and RNA deamination. Nature Reviews Genetics *23*, 505-518. 10.1038/s41576-022-00459-8.

102. Ruiz, P.D., and Smogorzewska, A. (2024). Temporary HMCES-DNA cross-link prevents permanent DNA damage. Cell Rep *43*, 113594. 10.1016/j.celrep.2023.113594.

103. Mohni, K.N., Wessel, S.R., Zhao, R., Wojciechowski, A.C., Luzwick, J.W., Layden, H., Eichman, B.F., Thompson, P.S., Mehta, K.P.M., and Cortez, D. (2019). HMCES Maintains Genome Integrity by Shielding Abasic Sites in Single-Strand DNA. Cell *176*, 144-153.e113. 10.1016/j.cell.2018.10.055.

104. Thompson, P.S., Amidon, K.M., Mohni, K.N., Cortez, D., and Eichman, B.F. (2019). Protection of abasic sites during DNA replication by a stable thiazolidine protein-DNA cross-link. Nat Struct Mol Biol *26*, 613-618. 10.1038/s41594-019-0255-5.

105. Rua-Fernandez, J., Lovejoy, C.A., Mehta, K.P.M., Paulin, K.A., Toudji, Y.T., Giansanti, C., Eichman, B.F., and Cortez, D. (2023). Self-reversal facilitates the resolution of HMCES DNA-protein crosslinks in cells. Cell Rep *42*, 113427. 10.1016/j.celrep.2023.113427.

106. Mehta, K.P.M., Lovejoy, C.A., Zhao, R., Heintzman, D.R., and Cortez, D. (2020). HMCES Maintains Replication Fork Progression and Prevents Double-Strand Breaks in Response to APOBEC Deamination and Abasic Site Formation. Cell Rep *31*, 107705. 10.1016/j.celrep.2020.107705.

107. Thompson, P.S., and Cortez, D. (2020). New insights into abasic site repair and tolerance. DNA Repair (Amst) *90*, 102866. 10.1016/j.dnarep.2020.102866.

108. Srivastava, M., Su, D., Zhang, H., Chen, Z., Tang, M., Nie, L., and Chen, J. (2020). HMCES safeguards replication from oxidative stress and ensures error-free repair. EMBO Rep *21*, e49123. 10.15252/embr.201949123.

109. Dungrawala, H., Rose, K.L., Bhat, K.P., Mohni, K.N., Glick, G.G., Couch, F.B., and Cortez, D. (2015). The Replication Checkpoint Prevents Two Types of Fork Collapse without Regulating Replisome Stability. Mol Cell *59*, 998-1010. 10.1016/j.molcel.2015.07.030.

110. Liu, W., Krishnamoorthy, A., Zhao, R., and Cortez, D. (2020). Two replication fork remodeling pathways generate nuclease substrates for distinct fork protection factors. Science Advances *6*, eabc3598. doi:10.1126/sciadv.abc3598.

111. Roy, S., and Schlacher, K. (2019). SIRF: a single-cell assay for in situ protein interaction with nascent DNA replication forks. Bio-protocol *9*, e3377-e3377.

112. Donsbach, M., Dürauer, S., Grünert, F., Nguyen, K.T., Nigam, R., Yaneva, D., Weickert, P., Bezalel-Buch, R., Semlow, D.R., and Stingele, J. (2023). A non-proteolytic release mechanism for HMCES-DNA-protein crosslinks. The EMBO Journal *42*, e113360.